Calcium sensitivity and mechanics of diaphragm muscle fibers in hypertrophic cardiomyopathy

A thesis submitted to McGill University in partial fulfillment of the requirements of the degree of Master of Science

Department of Kinesiology and Physical Education

Faculty of Education

McGill University

Montreal, Quebec, Canada

June 2019

TABLE OF CONTENTS

ACKNOWLEDGEMENTS

I have several people I would like to thank for their assistance, direct and indirect, toward the completion of this thesis. I would first like to thank my supervisor Dr. Dilson Rassier for the opportunity to obtain my master degree in his laboratory. His guidance and expertise, as well as patience and understanding, were invaluable in the achievement of this project.

I would like to thank my colleagues in the McGill Muscle Physiology and Biophysics laboratory. Fabio Minozzo and Anju Philips for their methodological training. Ricky, Daren, Andrea, Cheng, Rez and Oleg for their support – both technical and emotional – over the course of this degree.

Finally I would like to thank my family and friends for their patience and support: I appreciate everything you do.

CONTRIBUTION OF AUTHORS

The experiments, data analysis and author of this manuscript was Caitlin MacEachen.

Training and oversight of experiments was done by Fabio Minozzo and Anju Philips.

Research design, data analysis and document writing were done with the guidance of Dr. Dilson Rassier.

LIST OF FIGURES

ABSTRACT

Rationale: There is evidence of respiratory dysfunction and diaphragm weakness in hypertrophic cardiomyopathy. However little is known about the mechanism that underlies this weakness at the muscle fiber level.

Objectives: (i) To test if diaphragm weakness is present in a rabbit model of hypertrophic cardiomyopathy due to underlying R403Q mutation in the β-myosin heavy chain (MHC) and (ii) to determine whether crossbridge kinetics or calcium sensitivity are responsible for this dysfunction.

Hypothesis: Our hypothesis is that the R403Q mutation in β-MHC is responsible for diaphragm muscle weakness caused by abnormal actin-myosin cycling kinetics and calcium dysregulation.

Methods: Diaphragm muscle was dissected from rabbit with R403Q mutation and age-matched control and chemically permeabilized. Individual muscle fibers were isolated and mounted between a force transducer and a length controller, in temperature-controlled chamber. Fibers were submerged in maximal (pCa 4.5) and submaximal (pCa 4.7, 5.0, 5.2, 5.5, 5.7, 6.2, 6.5) activating solutions to elicit isometric contractions followed by a shortening-stretch protocol to measure rate of force redevelopment, a putative measurement of crossbridge kinetics.

Results: Maximum isometric force of R403Q fibers (58.1 ± 11.5 mN/mm^2) was only 61.3% that of WT fibers (94.8 ± 14.2 mN/mm^2). The rate of force redevelopment of R403Q fibers (k_{tr} = 3.31 ± 0.76 s^{-1}) was not significantly different from WT fibers (k_{tr} = 1.89 ± 0.28 s^{-1}) (p=0.15). Calcium sensitivity, measured as pCa_{50} and Hill's slope of force plotted over pCa, was not different between R403Q (pCa_{50} 4.39 ± 0.87, Hill's slope 5.15 ± 2.51) and WT (pCa_{50} 4.98 ± 0.35, Hill's slope 2.74 ± 0.66) fibers (p=0.22 and p=0.97 respectively).

Conclusions: Diaphragm fibers taken from rabbit with R403Q mutation exhibit weakness, but crossbridge kinetics and calcium sensitivity are not responsible for such dysfunction.

RESUME

Justification: C'est avec évidence qu'il y a une dysfonction respiratoire et une faiblesse du diaphragme dans la cardiomyopathie hypertrophique. Par contre, on ne sait pas le mécanisme causant cette faiblesse au niveau de la fibre musculaire.

Objectifs: (i) De vérifier si la faiblesse du diaphragme est présente dans un model de lapin pour la cardiomyopathie hypertrophique causé par la mutation R403Q dans le β isoforme du chaine lourde de myosine (β-MHC), et (ii) de déterminer si les cinétiques de cycle de l'interaction myosine-actine ou la sensibilité au calcium provoque cette dysfonction.

Hypothèse: Notre hypothèse est que la mutation R403Q dans la β-MHC est responsable pour la réduction de force des fibres musculaires du diaphragme causé par des altérations dans les cinétiques de cycle de l'interaction myosine-actine et la sensibilité au calcium.

Méthodes: Le diaphragme a été disséqué du lapin avec la mutation R403Q et d'un contrôle du même age et perméabilisé chimiquement. Des fibres individuelles ont été isolé du muscle et ont été attaché entre un transducteur de force et un contrôleur de longueur dans un bain avec une température réglée. Les fibres ont été submergé dans des solutions d'activation maximale (pCa 4.5) et sous-maximale (pCa 4.7, 5.0, 5.2, 5.5, 5.7, 6.2, 6.5) afin d'éliciter des contractions isométriques suivis d'un protocole de raccourci-étire pour mesurer la vitesse de redéveloppement de force, qui sert pour une mesure putative des cinétiques de cycle de l'interaction myosine-actine.

Résultats: La force isométrique maximale des fibres R403Q (58.1 ± 11.5 mN/mm^2) était seulement 61.3% de celle des fibres contrôles (94.8 ± 14.2 mN/mm^2). La vitesse de redéveloppement de force des fibres R403Q (k_{tr} = 3.31 ± 0.76 s^{-1}) n'est pas different celle des

fibres contrôles (k_{tr} = 1.89 ± 0.28 s^{-1}) (p=0.15). La sensibilité au calcium, mesuré par la pCa_{50} et le coefficient Hill h de la force en fonction de la pCa de la solution, n'a pas démontré de différence entre les fibres R403Q (pCa_{50} 4.39 ± 0.87, coefficient Hill 5.15 ± 2.51) et contrôles (pCa_{50} 4.98 ± 0.35, coefficient Hill 2.74 ± 0.66) (p=0.22 et p=0.97).

Conclusion: Les fibres du diaphragme du lapin avec la mutation R403Q ont démontré de la faiblesse mais les cinétiques de cycle de l'interaction myosine-actine et la sensibilité au calcium ne sont pas responsables pour cette dysfonction.

CHAPTER I:

LITERATURE REVIEW

INTRODUCTION

Skeletal muscles in the human body have specific properties related to the function it performs for movement or physiological regulation. Typically, a skeletal muscle is outlined by epimysium connective tissue which connects to, and is continuous with, tendons which transfer force to bones of the skeleton. Within the muscle, bundles of muscle cells – or muscle 'fibers' – are further delineated by perimysium connective tissue to form fascicles. Fascicles allow the enclosed fibers to work as a unit and collectively exert more force during contraction than they would be able to exert individually. The pattern of arrangement of fascicles within the whole muscle allow them to be specialized for different functions (OpenStax, 2016; Widmaier et al., 2006).

Muscle fibers are the units where muscle activation and contraction occur. Muscle fibers are long multinucleated cells, a result of the fusion of many precursor embryonic myoblasts (Mintz & Baker, 1967). Each muscle fiber is connected to a motor neuron which activates the contraction machinery within the myofibril via a process known as excitation contraction coupling. Myofibrils are the contractile elements within muscle fibers. When aligned, myofibrils form a series of alternating light and dark bands that give the muscle fiber its characteristic striated appearance. Each myofibril is composed of sarcomeres connected in series. Myofibrils are additionally connected with each other in parallel by structural proteins.

Muscle: Sarcomere and Myosin

The sarcomere, shown in figure 1, is the basic structural unit of muscle contraction. Each sarcomere contains a bipolar array of thick filaments, extending from each side of the central M-line to interdigitate with sets of thin filaments, in turn anchored to Z-lines. Z-lines delineate individual sarcomeres and connect them in series. The thin filaments are comprised primarily of

actin and form the light I band. Associated with actin, troponin and tropomyosin proteins have important functions in the activation and regulation of contraction at the sarcomere level. The thick filament is composed mainly of myosin, a molecular motor ultimately responsible for muscle contraction. The dark A band of the sarcomere is composed of the thick filaments as well as the area of overlap between the thick and thin filaments. Within the A band there is a slightly lighter band around the M-line in which there is no overlap with thin filaments, referred to as the H zone. The thick filament measures about 1.6µm while the thin filament ranges between 1.0-1.3µm for a total resting sarcomere length of about 2.5µm. However the length of the thick filaments is dependent upon the species and muscle type (Littlefield & Fowler, 2008).

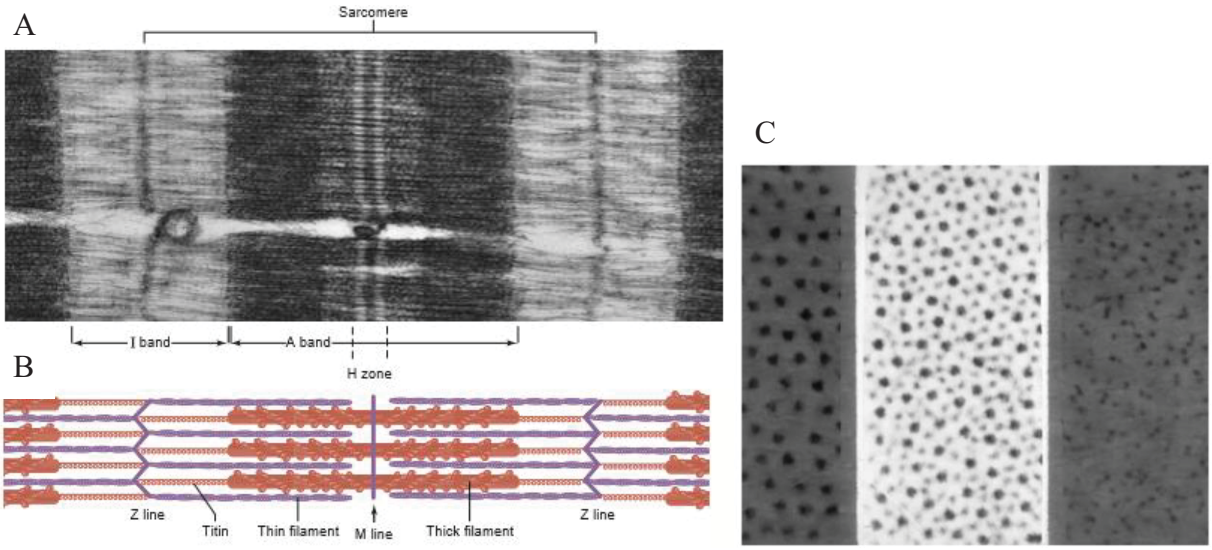

Figure 1: Image and diagram representations of skeletal muscle sarcomere. (*A*) Image of sarcomere within myofibrils. (*B*) Diagram representation of thick and thin filaments overlapping in the sarcomere. (*C*) Electron micrograph of sarcomere cross-section at H-zone (left, shaded showing thick filaments only), overlap zone (center with both thick and thin filaments in double-array organization), and I-band (right shaded, showing thin filaments only). Figures A and B adapted from (Widmaier, Raff, & Strang, 2006), figure C adapted from (Huxley, 2004)

Structural elements of the sarcomere include the proteins comprising the Z-lines and the M-lines, as well as the large elastic protein Titin. The Z-line consists of a dense network of

interconnected proteins that runs perpendicular to the thin filaments, maintaining their position and spacing, and extends beyond the myofibril to connect with sarcomeres of adjacent myofibrils. The Z-line therefore enables the transmission of lateral and longitudinal force within and between myofibrils during contraction (Wang & Ramirez-Mitchell, 1983). The M-line marks the midline of the sarcomere and serves as an anchoring point for the thick filaments. The M-line also connects titin with myosin and helps stabilize and maintain the alignment and spacing of thick filaments in the center of the sarcomere (Katzemich et al., 2012).

Titin is a large (3-4MDa) elastic protein that extends the full distance between the Z- and M-lines of the sarcomere (Labeit & Kolmerer, 1995). The N-terminal of titin spans the Z-line region (Gregorio et al., 1998) and overlaps with titin filaments from adjacent sarcomeres. Titin filaments additionally overlap in the M-line, and therefore form a contiguous system between sarcomeres along a myofibril. The central segment of titin, located in the I band, is an elastic region and extends to generate titin-based passive force during stretch. Alternative splicing of titin leads to the existence of several isoforms of this protein with differing lengths of this elastic region that may impart differences in passive stiffness and could affect contractile performance (Dos Remedios & Gilmour, 2017; Greising et al., 2012; Prado et al., 2005).

A cross sectional view of the sarcomere, such as that in figure 1c, reveals a double hexagonal array of filaments. Each thick filament can be seen to be surrounded by a hexagonal array of six thin actin filaments, with each thin filament being surrounded by a triangular arrangement of thick filaments. With an overall 2:1 thin to thick filament ratio, this arrangement maximizes binding opportunities for myosin head crossbridges to thin filaments in the region of overlap between filaments (Huxley, 1953, 1963, 2004).

Myosin is a molecular motor that binds to actin to drive muscle contraction. Myosin II is a heterohexamer that consists of two heavy chains and four light chains (two essential and regulatory). The C-terminus of the heavy chains dimerize into a helical tail (that binds the light chains) while each N-terminal forms a globular head, the myosin's motor domain, with an ATPase and actin binding sites (Cooke, 1995; Rayment, Holden, Sellers, Fananapazir, & Epstein, 1995; Ruff, Furch, Brenner, Manstein, & Meyhöfer, 2001). Myosin uses chemical energy stored in ATP to generate force and drive non-processive stepping along actin filaments. During each ATP hydrolysis cycle a myosin head binds to actin and generates one or several conformational changes with an overall displacement amplitude (step size) of ~5 nm or larger (Finer, Simmons, & Spudich, 1994; Kitamura, Tokunaga, Iwane, & Yanagida, 1999).

Mechanisms of Contraction

2.1 Sliding filament theory and crossbridge model of contraction

The sliding filament theory, proposed in 1954 (Huxley & Niedergerke, 1954; Huxley & Hanson, 1954), was based on the observation that the I band of the sarcomere decreased in size, while the A band did not change, as muscle fibers and myofibrils shortened during contraction. Such decrease was not due to proteins folding, but sliding of one filament over another.

The crossbridge model of contraction involves myosin heads extending from the thick filament to bind to actin, generating a 'power stroke' where actin is pulled relative to the thick filament. The myosin head then detaches before repeating the entire cycle. Crossbridges, or probably the heavy-meromyosin subunit of the myosin molecule are the basic units of force generation within the sarcomere (Huxley, 1957, 1969, 1973).

Huxley's 1957 theory involves crossbridges cycling between two functional states (shown in figure 2): a force generating state where myosin is bound to actin and a non-force generating state where myosin is unbound from actin. Huxley's theory includes a set of rate constants for the attachment and detachment kinetics between these states as a function of the crossbridge equilibrium position relative to its nearest attachment site on actin (depicted in figure 3a). Huxley's model for contraction was able to accurately predict force production from Hill (1938)'s earlier study, and proved to be an important tool in explaining isometric force production as a function of sarcomere length (Gordon et al., 1966).

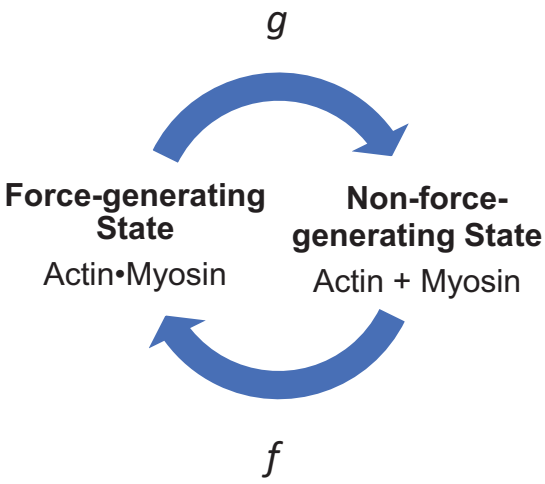

Figure 2: Two-state simple model of contraction, based on Huxley's original mechanism of crossbridge contraction. Figure adapted from (Huxley, 1957).

Further details about the conformation change that myosin heads undergo to perform the powerstroke were provided in subsequent studies. It was proposed that crossbridges transition through multiple states to generate force via the molecule's rotation (Huxley & Simmons, 1971; Huxley, 1969) (figure 3b). Determination of the crystalline structure of the myosin head (S1 region) revealed that it was a 'back door' enzyme, and further elucidated the mechanism by

which ATP binding myosin leads to actin dissociation and force production (Rayment et al., 1993) (figure 3c).

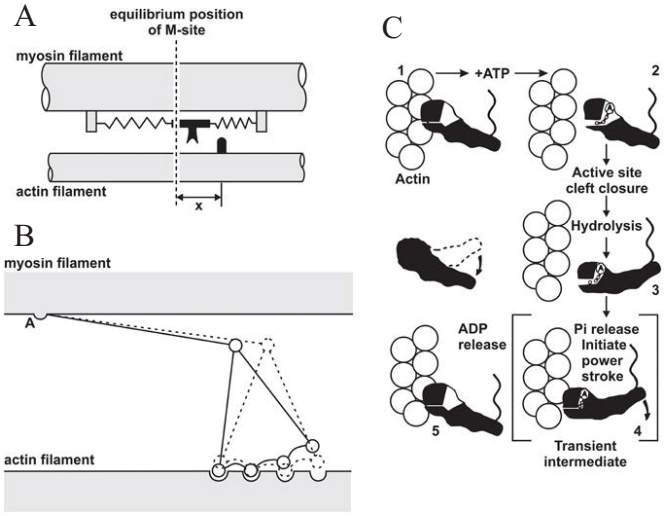

Figure 3: Evolution of crossbridge theory. (*A*) (Huxley, 1957) original thermal oscillation-driven model. (*B*) Multiple step and rotating head mechanism described by (Huxley, 1969) and (Huxley & Simmons, 1971). (*C*) (Rayment et al., 1993) description of contractile cycle incorporating structural features of the myosin head and actin binding sites. Figure adapted from (Herzog, Powers, Johnston, & Duvall, 2015).

The interaction of actin with myosin to generate force still generates controversy within the muscle field, and the crossbridge theory continues to be amended and expanded – for example, in 2016 Houdusse & Sweeney published an updated eight-state model of the chemomechanical cycle of crossbridge theory (Houdusse & Sweeney, 2016). However, simplified models of crossbridge theory still provide useful frameworks for problem solving and conceptualizing muscle behavior (Masataka & Halvorson, 2008; Palmer et al., 2007).

2.2 Simplified models of contraction: 2-state and 3-state crossbridge cycle

In the simple two-state model, force generation depends on the number of myosin heads (n) in parallel per half sarcomere (volume of a muscle fiber), the average force per crossbridge

(F) and the fraction of the total number of myosin heads that are strongly bound to actin in a force generating state (α_{fs}).

$$Force = nF\alpha_{fs}$$

Because an increase in fiber diameter (and cross-sectional area) leads to an increase in the number of myosin heads per half-sarcomere in parallel, the force generating capacity of that fiber also increases. To account for this (and allow assessment the intrinsic force-generating capability of the sarcomere), the force generated by a fiber during experiments is often normalized by its cross-sectional area and termed the specific force. This measure allows standardized comparison between fibers of different diameters. Muscle weakness at the fiber level, which can occur under a variety of conditions, is reflected by a decrease in specific force and is not just a result of muscle atrophy, where the decrease in force would be a result of a proportional decrease in cross-sectional area.

Another version of the model, shown in figure 4, incorporates three states and distinguishes between stages of crossbridge attachment and force generation. Addition of the third state, a weakly-bound state preceding the powerstroke and force production allows crossbridge detachment to be uncoupled from the completion of the ATPase cycle. This model has been useful for understanding transient behavior and delayed tension in muscle (Julian, Sollins, & Sollins, 1974).

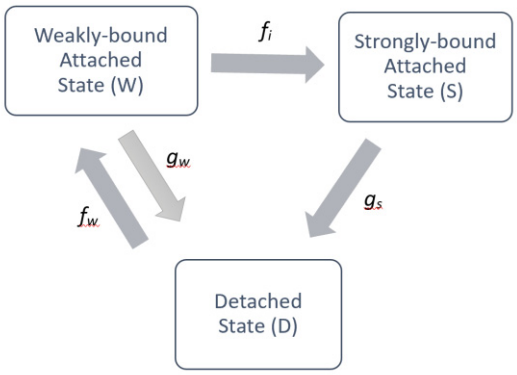

Figure 4: Three state model where D is a detached (non-force generating) state, W is a weakly-bound (non-force generating) attached state and S is a strongly-bound (force-generating) attached state. f_w is the rate at which crossbridges attached to form weakly-bound conformation (W) while g_w is the rate at which W-state crossbridges detach to return to the D conformation. f_i is the rate at which W-state crossbridges will transition to S-state (force-generating) crossbridges, while g_s is the rate at which crossbridges will detach from the strongly-bound conformation to return to detached state. This model is strain independent. Figure adapted from (Potma, van Graas, & Stienen, 1995).

2.3 Length-tension relationship

An important complement of the sliding filament and crossbridge theories is the length-tension relationship of muscle contraction (Gordon et al., 1966). This relationship links the structure of the sarcomere with the force produced during isometric contraction, and describes force production as a function of thick and thin filament overlap, and consequently the number of myosin heads available to bind actin and form crossbridges to generate force. This relationship is shown in figure 5.

The so-called descending limb of the force-length relationship, beginning at a sarcomere length 3.65 μm (corresponding to a position where thick and thin filaments are end to end and therefore not overlapping) up to sarcomere length 2.25 μm (region of complete filament overlap and the start of the force plateau), shows a linear relation between force and overlap, as sarcomere length decreases, filament overlap increases, and force increases. This infers a direct

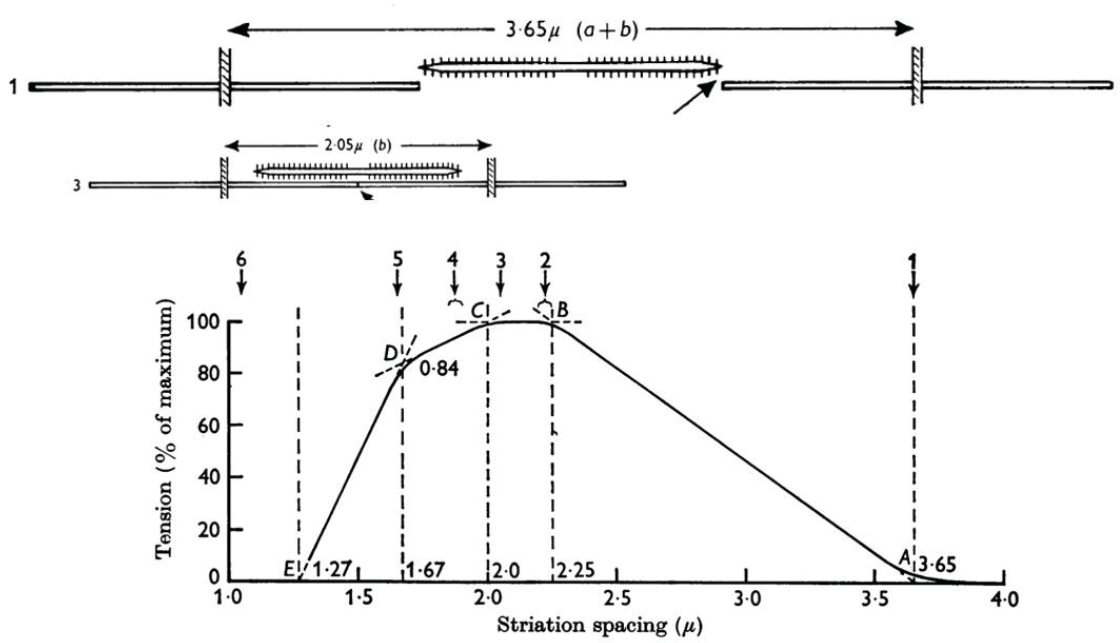

Figure 5: Length-tension relation with arrows pointing out critical stages of overlap of the filaments where distinct changes in the slope of force/striation spacing occur. 3 corresponds to the start of maximum overlap while 1 corresponds to the end of overlap between the filaments, and therefore the end of active force production. Schematic diagrams of the thin and thick filament overlap are overlain above the graphic. *a* corresponds to the length of the thick filaments (1.6μm) while *b* corresponds to the length of the thin filaments (2.05μm), as per (Page & Huxley, 1963). Adapted from (Gordon et al., 1966).

proportional relationship between the number of myosin heads exposed to the thin filament and the amount of force produced.

The force plateau (2.05-2.20μm for frog striated muscle used in this study) corresponds to a range of sarcomere lengths where there is optimal filament overlap (maximum crossbridge exposure and therefore maximum force production), and within which changes in sarcomere length do not appear to have an effect on force output. This is experimentally useful because it corresponds to a fiber's maximum force output and allows for small deviations in sarcomere length, bound to happen in an experimental setup.

The fiber preparations used in the study performed by Gordon et al. (1966) (as well as subsequent studies, e.g. (Edman, 1966)) involved the use of length-clamped segments of the fibers that were 7-10mm in length, and susceptible to intrinsic nonuniform sarcomere shortening disparities which might affect force outputs. Edman & Reggiani performed a renewed study investigating the length tension relationship in isolated frog muscle fibers with a technique that permitted the manipulation and measurement of short marked segments of 0.5-0.7mm of a fiber for the evaluation of isometric force and velocity of shortening (Edman & Reggiani, 1984, 1987). This length-tension relationship, shown in figure 6, differed from that of Gordon et al. (1966) in that it showed a smoother shape (without distinct corners such as Gordon et al.'s polygonal curve), with no distinct plateau between 2-2.2μm and a slightly sigmoid shape along the descending limb, which extrapolated to a shorter sarcomere length (3.49 vs 3.65). Despite these differences, this new length tension curve is still in agreement with the predictions of the sliding filament theory.

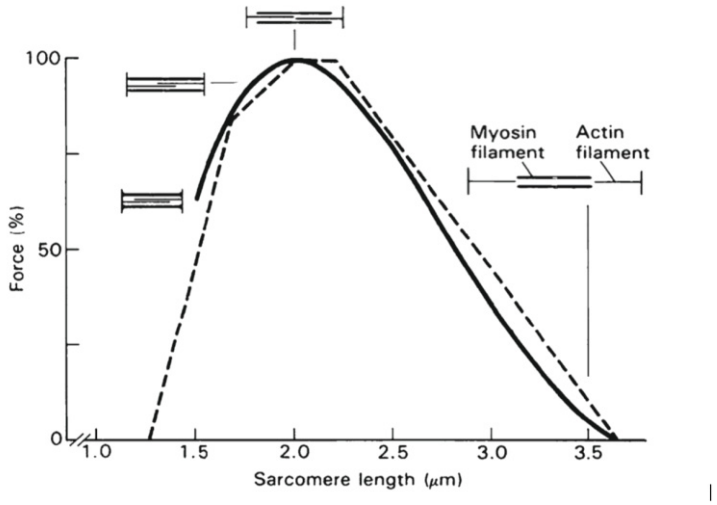

Figure 6. Solid smoothed length-tension curve from (Edman & Reggiani, 1987) measured with short length-controlled segments of single fibers, displayed next to the dashed polygonal curve from (Gordon, Huxley, & Julian, 1966). Inset are the corresponding thick and thin filament overlap diagrams. Adapted from (Rassier, 2010).

2.4 Brenner's Model/ Framework

Brenner and Eisenberg (1986) proposed a simple analytic framework based on Huxley's 2-state model to describe the transduction of chemical to mechanical energy during the crossbridge cycle. In this framework (shown in figure 7a) the transitions between the functional states can be described by two rate constants: f_{app} describes crossbridge attachment (transition from non-force generating state to force generating state) while g_{app} describes crossbridge detachment (transition from force-generating state to non-force generating state). In Brenner's model, non-force generating state encompasses myosin that is unattached to actin as well as myosin that is in a weak-binding conformation (with ATP or ADP•P_i bound) – which attaches and detaches from actin very quickly (Eisenberg & Hill, 1985; Stein, Schwarz, Chock, & Eisenberg, 1979). Brenner developed an experimental technique to detach all (or most) strongly bound crossbridges from an activated fiber to be able to measure their rate of attachment and force generation, without the confounding effects of the thin filament calcium (Ca^{2+}) activation (Brenner & Eisenberg, 1986) (shown in figure 7b). This experiment correlated the rate of force redevelopment with the rate limiting step in the ATPase cycle (Stein, Chock, & Eisenberg, 1984), a single order exponential supported by a rate constant of similar magnitude predicted by

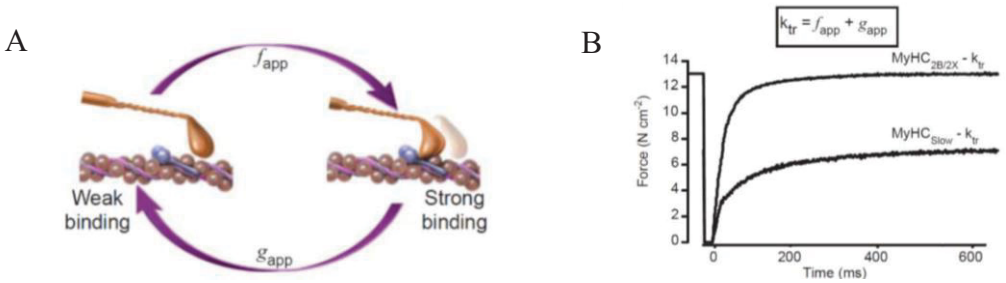

Figure 7: Brenner's two state framework and its experimental application. (*A*) Brenner two-state crossbridge kinetics framework. (*B*) Brenner's two-state framework to interpret crossbridge kinetic information from the rate of force redevelopment experiment. Adapted from (Greising et al., 2012).

a Huxley-type crossbridge model. This model also predicts that the rate of force development, determined by the rate of crossbridge attachment *f*, is significantly smaller than the rate constant for detachment of crossbridges at the end of their cycle *g*.

In this framework, the steady-state fraction of strongly-bound crossbridges in the force generating state (α_{fs}) is given by

$$\alpha_{fs} = \frac{f_{app}}{(f_{app} + g_{app})}$$

Campbell (1997) introduced a third state to this framework to account for crossbridge transition from non-cycling to cycling states (k_{on}, k_{off}) and thus the concept of crossbridge activation involving contributions from regulatory mechanisms of the thin filament proteins and Ca^{2+} binding, as well as from myosin cooperativity. This is shown in figure 8. Cooperativity is a process by which strongly-bound crossbridges influence further crossbridge activation and strong

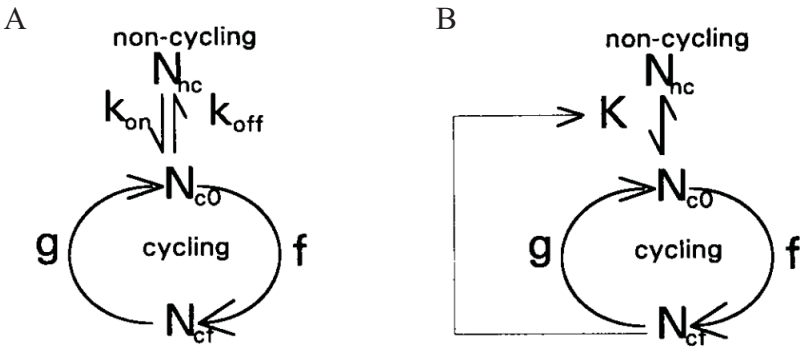

Figure 8: Campbell's three state framework includes an activation component, where crossbridges can transition between non-cycling (N_{nc}) and cycling (but not force-bearing, N_{c0}) states at rates k_{on} and k_{off}. As in earlier models, rates *f* and *g* represent the cycling from non-force-bearing (activated, N_{c0}) to force-bearing (N_{cf}) states and vice versa, respectively. (*A*) Shows activation of thin filament regulatory proteins (governed by k_{on}, k_{off}) and cycling of crossbridges. (*B*) Rates of activation, k_{on} and k_{off}, are considered to be fast relative to the rates of cycling, *f* and *g*, and are therefore replaced with K, an equilibrium activation factor. Feedback arrow between N_{cf} and K indicates cooperativity between force-bearing state and activation. Adapted from (Campbell, 1997).

binding for force production. This process (Campbell 1997 model results) enhances both activation and formation of more force-bearing crossbridges, and therefore force production, although it slows force (re)development. Cooperativity shows greatest enhancing effects at low Ca^{2+} activation and exhibits dynamic effects at varying range of Ca^{2+} concentrations.

2.5 Force-Velocity relationship

There is an inverse relationship between the force generated by muscle and its velocity of shortening (Fenn & Marsh, 1935; Hill, 1938). Hill's conceptual framework was based on thermodynamics, describing the force-velocity relationship as a rectangular hyperbola and highlighting its importance for understanding the underlying mechanisms of muscle contraction. Accordingly, the velocity decreases exponentially as the load, or force produced, increases (shown in figure 9). At one end of this relationship there is an isometric contraction, in which no shortening occurs (velocity = 0) and maximum force is produced. At the other extreme of this relationship is the maximum velocity (V_{max} or V_o), a theoretical 'unloaded' condition where there is no load opposing shortening, or force produced, and the maximal velocity is attained. Since V_{max} cannot be directly experimentally measured, it is therefore extrapolated from a curve of finite values or from different indirect protocols, such as the slack test (Claflin & Faulkner, 1985; Edman, 1979; Reggiani, 2007). V_{max} represents the maximum rate of cycling of the myosin crossbridges, and shows a linear relationship with the maximum rate of ATP hydrolysis (ATPase activity) of the contractile system (Bárány, 1967; Edman, 1988). The maximum rate of crossbridge cycling is independent of the number of bound crossbridges, and therefore the amount of filament overlap, as well as the degree of activation of the contractile system (twitch vs tetanus, sarcoplasmic reticulum pCa) (Edman, 1979).

The rate of ATP hydrolysis, linked with crossbridge detachment (g_{app}) – the rate limiting step of the crossbridge cycle – determines the cycling rate of individual crossbridges. The cycling rate of these crossbridges in turn determines the velocity of shortening. Increased load placed on a cross-bridge slows its forward movement during the power stroke, resulting in reduced overall rate of ATP hydrolysis and a decreased velocity of shortening (Widmaier et al., 2006). Thus the biochemical rates of crossbridge cycling are strain-dependent. This is in agreement with the well-established principle in muscle contraction that ATP hydrolysis increases in proportion to work performed – the Fenn Effect (Fenn, 1923). The rate of ATP hydrolysis for an isometric contraction is therefore less than the ATP hydrolysis at V_{max}.

The force generated by a muscle depends on the total number of crossbridges attached to actin. Because it takes a finite amount of time for crossbridges to attach, as filaments slide past one another faster and faster (i.e., as muscle shortens with increasing velocity), the window of opportunity for crossbridge attachment decreases, resulting in fewer crossbridge binding events and reduced force production (Huxley, 1957).

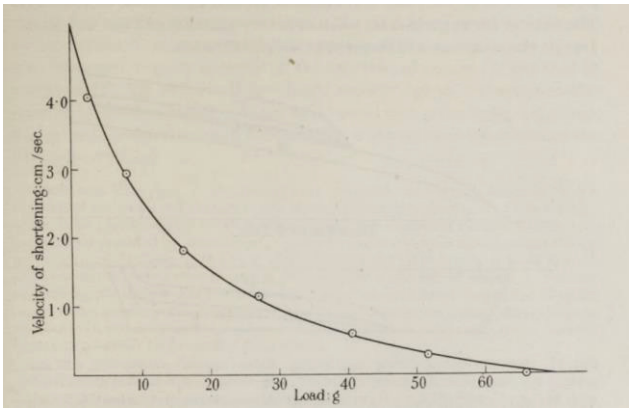

Figure 9: Force-velocity relationship shows exponential decrease in velocity as the force, or load, is increased. This curve demonstrates the relationship between load (in grams) and speed of shortening (cm/s) in isotonic contraction. Adapted from (Hill, 1938).

2.6 Passive Force – Length relationship

The passive tension generated by a muscle that is stretched also exhibits length dependence. When a muscle fiber at rest is stretched beyond its resting length (L_o), it displays viscoelastic properties and its tension increases at an exponential rate as the sarcomere length is increased (figure 10a) (Gordon et al., 1966; Hill, 1968; Proske & Morgan, 1999). Titin, the giant elastic protein, is considered the primary determinant of passive stiffness (Prado et al., 2005; Wang, McCarter, Wright, Beverly, & Ramirez-Mitchell, 1991). It has been proposed that weakly bound crossbridges contribute to passive tension (Campbell & Lakie, 1998; Granzier & Wang, 1993), however this remains a matter of debate (Bagni, Cecchi, Colomo, & Garzella, 1992; Bartoo, Popov, Fearn, & Pollack, 1993; Mutungi, 2003; Proske & Morgan, 1999). The relationship between passive tension and sarcomere length can vary across muscles and species (figure 10b shows the interplay of active and passive tension as a function of sarcomere length).

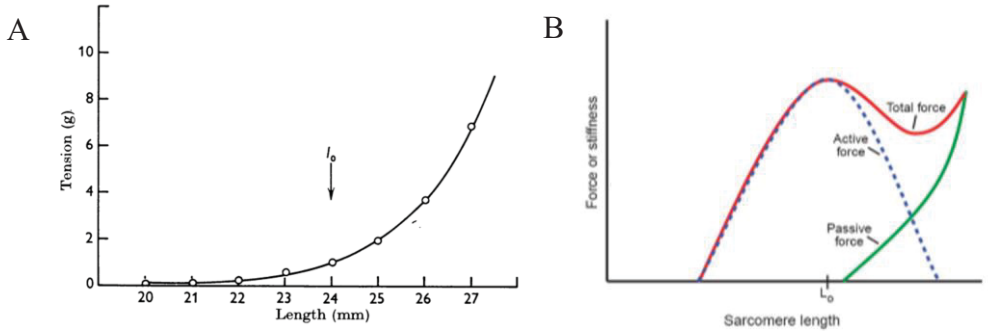

Figure 10. Passive force – length relationship. (*A*) Force increases exponentially as muscle is passively lengthened. Adapted from (Hill, 1968) (*B*) Total force of muscle is a summation of the active and passive forces produced as a function of sarcomere length (relative to L_o of a given muscle). Adapted from (Greising, Gransee, Mantilla, & Sieck, 2012).

2.7 Ca^{2+} activation and thin filament regulation of contraction

The activation of the sarcomere contraction by Ca^{2+} is regulated by a complex of thin filament accessory proteins troponin and tropomyosin. Troponin is composed of three subunits (T, I and C). At rest, troponin and tropomyosin, a long chain-like protein, sit along actin sterically blocking its myosin binding sites (Fujii, Iwane, Yanagida, & Namba, 2010; Ohtsuki, Masaki, Nonomura, & Ebashi, 1967; Spudich, Huxley, & Finch, 1972). When Ca^{2+} is released into the myoplasm, it binds troponin C (TnC) which causes a conformation change in the T and I subunits and shifts tropomyosin to expose myosin binding sites along the actin filament (Lehman, Craig, & Vibert, 1994). Thus, Ca^{2+} allosterically activates the thin filament to increase the probability of crossbridge formation by removing steric hindrance of the troponin-tropomyosin complex.

2.8 Excitation-contraction coupling

The motor neuron transmits an action potential, causing a depolarization of the presynaptic nerve terminal and a release of acetylcholine (Ach). Ach binds to cholinergic receptors in the post-synaptic motor endplate, triggering depolarization and an action potential that is propagated along sarcolemma of the muscle fiber and into folds that extend within the fiber to the myofibrils via transverse (t-) tubule network. These activate voltage-gated Ca^{2+} channels within the t-tubules, known as DHPR or dihydropyridine receptor channels, which further allosterically activate the RyR ryanodine receptor channels of the sarcoplasmic reticulum (SR). Opening of the RyR channels, and release of Ca^{2+} from the sarcoplasmic reticulum, causes an increase in the myoplasmic Ca^{2+} concentration and allows activation of the Ca^{2+} regulated apparatus of the thin filament (Flucher & Franzini-Armstrong, 1996; Franzini-Armstrong, 1970; Huxley & Taylor, 1958).

The increase in Ca^{2+} concentration is only transient as it is immediately returned to the SR via SERCA active pumping mechanism. Phosphorylation of the SERCA-associated protein phospholamban provides additional Ca^{2+} regulation, increasing the rate of SERCA's Ca^{2+} uptake activity when in a phosphorylated state (Periasamy & Kalyanasundaram, 2007). Calsequestrin, another SR protein, additionally binds free Ca^{2+} in the SR (Franzini-Armstrong & Jorgensen, 1994), reducing the 10 000-fold [Ca^{2+}] gradient between the SR and the myoplasm and facilitating the SERCA pump against this gradient. Ca^{2+} is thus highly regulated and is used as a precise signaling molecule in muscle contraction.

Experimental variables and methodology

3.1 Index of crossbridge kinetics: Rate of force redevelopment (k_{tr})

There are many experimental conditions where it is desirable to be able to assess the sensitivity of crossbridge kinetics to various factors and treatments. Brenner's two state model provides a framework to assess crossbridge kinetics as a measurement of the rate that crossbridges transition from a weak to a strongly-bound force generating state (f_{app}). This rate can be estimated by a well-established procedure (Bates et al., 2013; Brenner & Eisenberg, 1986; Brenner, Yu, Greene, Eisenberg, & Schoenberg, 1986; Kreutziger et al., 2008; Sweeney & Stull, 1990). Upon maximum activation, a fiber is mechanically shortened, allowing it to go slack and its force to momentarily drop to zero, followed by a restretch to its original length. This serves to detach strongly bound crossbridges, and after the restretch, the rate at which force redevelops reflects the rate at which crossbridges transition into a strongly bound force-generating state (Brenner, 1988; Gordon, Homsher, & Regnier, 2000). Important features of this experiment are the initial detaching of strongly bound crossbridges, preventing the crossbridge cycling rate-

limiting step of detachment (g_{app}), as well as performing it on a maximally activated fiber, thereby eliminating the time effects of the non-crossbridge activation.

The rate constant for force redevelopment (k_{tr}) is the experimental measure of interest in this protocol. It is calculated by fitting the force transient after restretch to a single exponential equation:

$$F = a(1 - e^{-ct}) + b$$

where *t* is time, *a* is amplitude of the exponential force development, *b* is the initial force value and *c* is the rate constant for force redevelopment k_{tr}.

This measure has been used experimentally to assess the sensitivity of crossbridge cycling to various conditions and treatments. The rate of force redevelopment is sensitive to the level of Ca^{2+} activation (Brenner, 1988; Metzger & Moss, 1990).

3.2 Myoplasmic Ca^{2+}-Force relationship: Hill coefficient, pCa_{50}

The relationship of force generation as a function of myoplasmic Ca^{2+} concentration, as a result of Ca^{2+} activation of the thin filament, is readily observed in permeabilized muscle fiber experiments. Such a preparation eliminates excitation contraction coupling and allows manipulation of the chemical milieu of the sarcomere directly (Roche, Gumucio, Brooks, Mendias, & Claflin, 2015).

There is a hyperbolic ($[Ca^{2+}]$) or sigmoid ($pCa = -\log[Ca^{2+}]$) relationship between Ca^{2+} and muscle force generation (Hellam & Podolsky, 1969; Weber & Murray, 1973). The resemblance of the relation to the 1910 Hill equation describing the cooperative binding of

oxygen to haemoglobin established the equation describing this relationship as the modified hill equation (Fabiato & Fabiato, 1975; Hill, 1910; Walker, Li, & Buttrick, 2010).

The modified hill equation:

$$\frac{P}{P_0} = \frac{1}{1+10^{h \cdot (pCa_{50} - pCa)}}$$

where P is the tension, P_0 is the maximum tension, *h* is the hill coefficient and pCa_{50} is the pCa required for half maximal force development. A strength of the hill equation is that it allows muscle physiologists to summarize results of these types of experiments in terms of two constants: hill coefficient (*h*) and pCa_{50}. The Hill coefficient is a measure of the 'steepness' (slope) of the predicted curve, and it reflects cooperativity in fiber activation and force generation. The pCa_{50} expresses the midpoint of the force-pCa curve and is interpreted as an index of Ca^{2+} sensitivity of the muscle fiber.

Hypertrophic cardiomyopathy

Hypertrophic cardiomyopathy (HCM) is the most common genetic cardiac disease affecting an estimated 1 in 500 people (Maron et al., 1995). It follows an autosomal dominant inheritance pattern (Greaves, Roche, Neutze, Whitlock, & Veale, 1987; Ho, 2010) of mutations in one or more genes encoding proteins of the cardiac sarcomere, most commonly affecting components of the molecular motor myosin (Ho, 2016; Seidman & Seidman, 2011). Mutations in cardiac β-myosin heavy chain (MHC) and myosin binding protein C are most common and are collectively responsible for 50% of HCM families (Marian & Braunwald, 2017) and over 80% of HCM cases with an identified genetic cause (Ho, 2012, 2016).

There is considerable diversity in the disease course, age of onset and severity of symptoms, and in the risk for progression to serious disease outcomes in HCM (Ho, 2010; Maron, McKenna, et al., 2003). The defining clinical characteristic of the disease is asymmetrical hypertrophy of the left ventricle and septum unexplained by secondary causes (Marian & Braunwald, 2017) while its pathohistological hallmark is interstitial fibrosis, myocyte disarray and capillary rarefaction (Güçlü et al., 2015; Ho, 2010; Velden & Stienen, 2019). Left ventricular outflow tract (LVOT) obstruction develops in the majority of cases (Elliott et al., 2006; Maron, Olivotto, et al., 2003; Maron et al., 2006) and may contribute to progression of symptoms such as pulmonary congestion and exertional dyspnea (Fatkin et al., 2000; Ho, 2010; Maron, Olivotto, et al., 2003; Sorajja et al., 2009). However there is also evidence of high LVOT gradients being well tolerated for extended periods of time (Cirino & Ho, 2014). Arrhythmias may also manifest with the disease, with atrial fibrillation developing in approximately 20–25% of patients, which may be associated with an increased risk of stroke and thromboembolic complications. Overall the most common symptom in HCM is shortness of breath, particularly during exertion, which is present in up to 90% of patients (Ho, 2010). While the majority of HCM patients will be able to manage their symptoms and maintain a normal life expectancy (Elliott et al., 2006; Maron, McKenna, et al., 2003), HCM can develop into a serious medical condition with risks including sudden cardiac death (SCD) and refractory heart failure (Ho, 2016). HCM is the lead cause of SCD in young people, particularly young athletes (Ho, 2010), and occasionally this may be the disease's first manifestation (Maron et al., 2000). A burnt-out end stage phase of HCM occurs in 5-10% of patients, accompanied by a deteriorating prognosis that includes increased risk of cardiovascular events and need for transplantation. This phase is marked by left ventricular systolic dysfunction, worsening of symptoms and occasionally left

ventricular wall thinning and chamber enlargement (Biagini et al., 2005; Harris et al., 2006; Ho, 2010).

Diagnosis of HCM is most often established through noninvasive cardiac imaging such as echocardiography or cardiac magnetic resonance imaging and can be further elucidated through pathognomonic histopathic testing and molecular genetic assessment (Cirino & Ho, 2014). Clinical evaluation may be triggered in response to symptoms, or in asymptomatic individuals after detection of a systolic murmur or abnormal electrocardiogram (ECG), or as a result of a family screening (Ho, 2010). However none of these assessments are part of a standard medical examination and therefore, unless a family history of familial HCM prompts an early investigation, clinical diagnosis usually only occurs in response to progressed disease symptoms. As a result, current treatment for this disease focuses on symptom management. There are currently no strategies to prevent or modify disease progression in asymptomatic (subclinical) patients (Ho, 2016).

4.1 Subclinical symptoms of disease

Despite the overt symptoms and serious outcomes associated with progressed HCM disease, many patients will live much of their lives with absent or mild clinical symptoms. Studies of HCM patients who are preclinical and otherwise appear asymptomatic provides important insight into the early mechanism of this disease, linking sarcomere mutation and molecular dysfunction to clinical outcomes. They are important for uncovering early therapeutic targets before progression to overt symptomatic disease state. Imaging of asymptomatic mutation carriers show diastolic dysfunction and myocardial inefficiency preceding the development of hypertrophy (Crilley et al., 2003; Ho & Seidman, 2006; Velden & Stienen, 2019). Additionally, ECG abnormalities (Lakdawala et al., 2011), mitral valve abnormalities (Captur, Flett, Jacoby, &

Moon, 2013), myocardial crypts (Brouwer et al., 2012; Germans et al., 2006; Maron, Maron, & Semsarian, 2012) and evidence of fibrosis (Ho, 2010; Ho et al., 2013) have also been identified as early preclinical phenotypes in the presence of normal ventricular wall thickness.

4.2 Early mechanisms of disease

Marian and Braunwald (2017) describe the pathogenesis of early HCM as complex and mutation specific, but broadly consisting of four interlocking sets of mechanisms. Primary mechanisms are the direct effects of the mutation on the structure and function of the sarcomere protein it encodes, and include changes in mRNA transcription, protein expression, sarcomere assembly, Ca^{2+} sensitivity, ATPase enzyme activity and force generation. Secondary mechanisms are molecular events in response to dysfunctions occurring in the primary mechanism, such as altered gene expression, and activation of signaling pathways, such as the MAPK and TGFB1 pathways. These events cause intermediary changes that are directly linked to characteristic tertiary and quarternary phenotypes and are thought to represent common maladaptive mechanism present in other forms of cardiac hypertrophic response. Tertiary phenotypes represent histological changes including myocyte hypertrophy, myocyte disarray, interstitial fibrosis, and cardiac hypertrophy, while quarternary phenotypes include clinical phenotypes: cardiac arrhythmias, SCD, LVOT obstruction, and heart failure (Marian & Braunwald, 2017).

4.3 R403Q mutation

The R403Q mutation, affecting the β-MHC of myosin, was the earliest and remains the best characterized mutation underlying HCM. Geisterfer-Lowrance et al. (1990) demonstrated that a missense point mutation of arginine to glutamine at position 403 of the MYH7 gene was

the underlying cause of a malignant form of familial HCM and subsequently established HCM as a ‘disease of the sarcomere’ (Lowey, 2002). Early development of animal models allowed a more direct evaluation of this mutation and its functional effects in the heart. Since then, it has been the most studied genetic mutation underlying HCM.

The MYH7 gene encoding the β-MHC is the predominantly expressed isoform in adult human ventricle (Marin-Garcia, 2007). Since the initial discovery of the R403Q mutation, >300 mutations in the β -MHC have been identified and this protein is affected in >30% of identified cases of HCM (Lowey et al., 2018; Spudich, 2014). Arg 403 is located in a highly conserved sequence in myosin II, and the loop structure that it encodes (known as the cardiomyopathy (CM) loop) appears the same in x-ray structures of myosin in both smooth and striated muscle. Ecken, Heissler, Pathan-Chhatbar, Manstein, and Raunser (2016) and Lorenz and Holmes (2010), through their respective cryo-EM mapping of the actomyosin complex, demonstrated that Arg403 does not interact directly with actin but with the opposing strand of the CM loop to stabilize its conformation and is of high importance for strong binding between actin and myosin.

There has been controversy in the literature as to the mechanism by which R403Q mutation affects actomyosin interactions and sarcomere function. Most prominently is the division between evidence for outcomes of this mutation being a loss of function (Ho, 2010) or gain of function (Hasenfuss, 1998; Spudich, 2014) phenotype. It is only recently that discrepancies in results between models have been elucidated, perhaps most importantly with the finding that the cardiac α-MHC isoform (presence in mouse and small rodent ventricle) differs in crucial ways from that of β-MHC present in humans and larger mammals (Lowey, Bretton, Gulick, Robbins, & Trybus, 2013; Lowey et al., 2008). Lowey et al. (2018), using a rabbit model

with endogenous cardiac β-MHC, showed a loss of function in both isolated molecules and ordered molecule experimental setups. In vitro motility assay showed reduced velocity of heterodimeric myosin molecules with no change in ATPase activity of the S1 head. Myofibrils (which maintain myosin in its native thick filament organization) showed reduced steady state isometric force production and reduced rates of force development, redevelopment and relaxation. The force-velocity relationship calculated for the myofibrils showed a decrease in shortening under load that ultimately resulted in diminished power output by the heart.

Additionally, homology between the β-MHC isoforms in cardiac and type I skeletal muscle means the R403Q mutation also occurs in skeletal muscle myosin. Cuda, Fananapazir, Zhu, Sellers, and Epstein (1993) conducted their study on soleus muscle of HCM patients with identified R403Q mutation because of the difficulty in cardiac sampling. Their study, and others (Cuda, Fananapazir, Epstein, & Sellers, 1997; Lowey et al., 2018; Palmiter et al., 2000), suggest a similar mechanism of dysfunction as that which occurs in cardiac β-MHC. Lowey et al. (2018) ran soleus myofibrils in parallel with their ventricle experiments and found nearly equivalent results, with reductions in all parameters for the R403Q group (isometric force, rate of development and redevelopment) except for an unchanged rate of relaxation. This weakness has been identified as an intrinsic dysfunction, a myopathy, and not a secondary effect due to atrophy or maladaptation to a dysfunctional or failing heart. This supports findings of perturbed skeletal muscle function in some patients with HCM, albeit without overt symptoms of myopathy (Caforio et al., 1989). Study of the dysfunction of slow skeletal muscle has been purported to give insight into the early disease pathology of cardiac muscle, prior to remodeling effects that occur with the disease (Lankford, Epstein, Fananapazir, & Sweeney, 1995).

4.4 Animal model to study mechanism of HCM R403Q mutation

Animal models are a staple of basic science and facilitate the study of specific disease features in a controlled environment. Establishment of the genetic basis of HCM has allowed appropriate models of this pathology to be created through genetic engineering. This type of research is particularly important for HCM because of the significant variation in human studies of the pathophysiology for a given mutation due to background genes and epigenetics, environment, lifestyle or other yet to be identified confounding variables (Fatkin et al., 2000; Ho, 2010; Seidman & Seidman, 2014). Family members with the same inherited causal mutation can show very different disease courses, underscoring the disconnect between genotype and clinical outcomes (Ho, 2010). Kirschner et al. (2005) suggested there is even variation in expression of mutated and 'wild type' protein between cells within a given individual. Animal models furthermore enable the collection of cardiac and diaphragm tissue samples, rarely available in human studies, and allow for collection at early ages, before the onset of secondary symptoms that obscure the primary disease (Seidman & Seidman, 2014).

A murine model was the first developed for HCM in 1996 for the R403Q mutation (Geisterfer-Lowrance et al., 1996). It was the first transgenic animal model developed for this mutation and appeared to capture the essential phenotype and pathogenesis of the human disease. However, results from some studies using this model have conflicted with human studies, most critically establishing a 'gain of function' paradigm to actomyosin interactions contrary to previous research, which had suggested a 'loss of function' (Cuda et al., 1997; Cuda et al., 1993; Fujita et al., 1997; Lowey, 2002; Sata & Ikebe, 1996; Sweeney, Straceski, Leinwand, Tikunov, & Faust, 1994)). α-MHC is the fast isoform of MHC, present in fast twitch human skeletal muscle as well as human atria while β-MHC is the slow isoform of MHC, present in slow twitch

skeletal muscle and cardiac ventricular muscle. Due to 93% homology in amino acid sequence between mouse and human ventricle cardiac α-MHC and β-MHC, respectively, it was assumed that there should be little or no difference in their function (Lowey et al., 2018). However small differences between the two isoforms can be found in regions implicated in functional importance, such as the surface loops 1 and 2 and the light chain binding domain (Lowey, 2002; McNally, Kraft, Bravo-Zehnder, Taylor, & Leinwand, 1989). Van Buren, Harris, Alpert, and Warshaw (1995) found that these differences led to a 2x greater ATPase activity and in vitro motility assay sliding velocity for α-cardiac myosin than β-cardiac myosin. Lowey et al. (2008) investigated this discrepancy using a transgenic mouse model where R403Q mutation was expressed in the native α-MHC backbone as well as in a β-MHC replaced backbone. The authors demonstrated an increase in the in vitro motility assay sliding velocity as well as ATPase activity. Therefore, the functional consequences of the mutation are fundamentally changed depending upon the context of the cardiac MHC isoform. This was further confirmed by a study showing transient kinetic differences in equilibrium constants and rates of nucleotide binding and release for the S1 isoform in α- and β-MHC transgened into a mouse model (Lowey et al., 2013).

Marian et al. developed a transgenic R403Q rabbit model in 1999 to address discrepancies between the human and mouse model of HCM (Marian et al., 1999). A lack of left ventricular hypertrophic response (Marian et al., 1999; Oberst et al., 1998) and impaired systolic function (Geisterfer-Lowrance et al., 1996; Marian et al., 1999; Muthuchamy et al., 1999; Oberst et al., 1998; Tardiff et al., 1998; Vikstrom, Factor, & Leinwand, 1996; Yang et al., 1998) observed in the mouse model contradicted fundamental aspects of the human disease. Significant differences had been observed between α- and β- MHC isoforms in terms of actin-activated-Mg-ATPase activity and crossbridge kinetics (Marian et al., 1999; Pagani, Shemin, & Julian, 1986; Schwartz

et al., 1981; Sugiura, Kobayakawa, Fujita, Momomura, et al., 1998; Sugiura, Kobayakawa, Fujita, Yamashita, et al., 1998). Later studies further confirmed these isoform and species differences (Alpert et al., 2002; Lowey et al., 2018; Malmqvist, Aronshtam, & Lowey, 2004). Rabbit myocardium had been found to be β-MHC dominant with approximately 98% homology to the human β-MHC protein (Jaenicke et al., 1990; Kavinsky et al., 1984; Marian et al., 1999). The R403Q mutation was transgened into the rabbit and the resulting phenotype was very similar to the human disease – showing premature death, cardiac hypertrophy, myocyte disarray, interstitial fibrosis and normal systolic function (Marian et al., 1999).

Nagueh et al. (2004) further examined the evolution of phenotypes over lifespan of the R403Q transgenic rabbit through a set of cross-sectional and longitudinal studies. In the cross-sectional study, rabbits were categorized into four age groups designed to reflect onset and important changes in phenotype of humans while the longitudinal study conducted follow ups in the same adult rabbits over the course of a year. For both studies, echocardiographic and tissue Doppler imaging were conducted in addition to histological (interstitial collagen volume fraction, myocyte disarray and cross-sectional area) and molecular evaluation (myofibrillar Ca^{2+} activated ATPase activity, detection and quantification of signaling kinases and molecules). Important findings from this study were the early reduction in Ca^{2+} sensitivity of myofibrillar ATPase activity in absence of other discernible phenotypes, the early and independent development of myocyte disarray, compared to hypertrophy and fibrosis, and the decrease in myocardial contraction and relaxation prior to change in histological phenotype and or global cardiac function. This study showed that the phenotype progress over lifetime of the transgenic rabbit resembled that of the human disease. Importantly, it also showed a disease progression prior to and independent of heart failure.

4.5 Diaphragm

The diaphragm is the primary pump muscle for breathing in humans. It is a sheet-like skeletal muscle enclosed by thick connective tissue that originates and runs from the sternum, lower ribs and vertebrae to a central membranous tendon. It contracts and flattens during inspiration and passively lengthens during expiration, serving as a dome-shaped separation between the abdominal and thoracic cavities. In doing so it acts to change transthoracic pressure, which changes lung volume, pulling air and oxygen in via negative pressure during inspiration and forcing it back out via passive compressive pressure during expiration. The diaphragm's function is essential for breathing under conditions of health and is an important determinant of respiratory mechanics. As the lungs are the site of oxygen and carbon dioxide exchange for the blood, proper respiratory mechanics are essential to maintain cardiovascular function. When the diaphragm is unable to meet the needs of the cardiovascular system, either due to intrinsic weakness or an increase in the imposed load resulting from physiological deficit or mismatch elsewhere in the body, dyspnea and disease can ensue.

The diaphragm is composed of type I (slow) and II (fast) fibers in humans (Polla, D'Antona, Bottinelli, & Reggiani, 2004). Difficulty in procuring diaphragm muscle samples in humans means that research on this topic is relatively scarce; studies that have examined diaphragm fiber composition are often not systematic, with limited biopsy collection and small sample size (Sieck, Ferreira, Reid, & Mantilla, 2013). The measures and estimates of fiber type distribution in the adult human diaphragm can vary between studies. Polla et al. (2004) estimate about 55% slow fibers, 21% fast oxidative (IIa), and 24% fast glycolytic (IIb) while Levine, Kaiser, Leferovich, and Tikunov (1997) similarly found 45%, slow fibers, 39% type IIa and 17% type IIb.

Slow fibers are the main drivers of quiet breathing, while fast fibers are recruited when breathing rate increases. Citterio, Sironi, Piccoli, and Agostoni (1983) studied the firing patterns of diaphragm muscle in rabbits at rest and during tachypnea (rapid breathing) and found a shift in recruitment from slow to fast muscle fibers. Ventilation rate increases inversely proportional to body size in mammals and also the proportion of fast fibers in respiratory muscles to meet this need. As a result, smaller mammals such as mice and rats have diaphragms with a higher proportion of fast fibers (Blank, Chen, & Ianuzzo, 1988; Hodge et al., 1997; Polla et al., 2004). Diaphragm samples from other species have also shown the presence of multiple fiber types in varying proportions (Sieck et al., 2013).

Diaphragm muscle fibers differ from other skeletal muscle fiber types for a number of characteristics. Diaphragm fibers generally have a smaller cross-sectional area than limb muscles but maintain the same capillary density, therefore decreasing the diffusion distance and increasing oxygen efficiency compared with other muscles (Green, Plyley, Smith, & Kile, 1989; Mizuno, 1991; Polla et al., 2004). The diaphragm also possesses specialized excitation contraction coupling features, specifically a more responsive isoform of the sarcoplasmic reticulum calcium release channel RyR3 (Bertocchini et al., 1997; Polla et al., 2004; Rossi, Bottinelli, Sorrentino, & Reggiani, 2001). These features of the diaphragm contribute to its ability to be constantly active without becoming fatigued.

4.6 Diaphragm dysfunction in cardiomyopathy and heart failure

A number of studies have found abnormalities in respiratory muscle under conditions of cardiomyopathy using a Syrian hamster model. Various strains of this model have been developed that mimic human disease phenotypes, such as for dilated (bio 53:58) and hypertrophic (bio 14:6) cardiomyopathy. Stassijns et al. (1999) reported reduced force-

generating capacity after correcting for fiber CSA, suggesting myopathy in the diaphragm of the bio 53:58 dilated cardiomyopathy strain. They reported lower fatiguability in diaphragm fibers and a fiber-type shift toward type 1 in the diaphragm, but not the gastrocnemius, accompanied by increased atrophy in type 1 fibers of both muscles. Lecarpentier et al. (1997) also found reduced force in the diaphragm due to decreased number of crossbridges in this model. Burbach, Schlenker, and Johnson (1987) examined skeletal muscle histology in the bio 14:6 hypertrophic strain and found an increase in absolute diaphragm weight, despite reduced gastrocnemius weight, and a reduction in the size of both type I and II diaphragm fibers in animals with 35 and 180 days of age. Jasmin and Proschek (1982) monitored changes in muscle of the UX-7.1 Syrian hamster (a subline of the bio 14:6 hypertrophic strain) throughout its lifetime (0-250 days). They describe necrotic lesions that occur first in respiratory muscles of the newborn animals before progressing to the rest of the skeletal musculature and the heart over time, suggesting that diaphragm weakness in animal model of hypertrophic cardiomyopathy is at least partly due to congenital myopathy in the muscles and not just due to secondary effects of the cardiomyopathy. The necrotic effects were most consistent and severe in the diaphragm muscle, compared to limb muscle, followed by other continually active muscles such as the intercostals and the tongue.

The diaphragm has received little attention in studies of HCM, compared with hypertrophic response in cardiac muscle (and other heart-centric changes) and accompanying myopathy in limb slow skeletal muscle. However early studies of experimental cardiomyopathy indicate that this may be a source of dysfunction worth pursuing in both animal models and humans. Evidence for the presence and potential mechanism of diaphragm weakness in HCM, and specifically HCM due to R403Q mutation, exists in studies that have examined primary

intrinsic skeletal myopathy due to mutation in β-MHC and diaphragm dysfunction that develops concurrently with or in response to dysfunctional hypertrophic heart and heart failure.

Early studies that established the genetic basis of cardiomyopathy as a mutation in the highly conserved MYH7 gene also recognized that due to overlap of protein expression in cardiac and skeletal muscle types, skeletal muscle β-MHC also exhibited this mutation. Caforio et al. (1989) found that, despite the predominant disease pathology being in the heart, skeletal function was perturbed in some but not all individuals with hypertrophic and dilated cardiomyopathy. Fananapazir, Dalakas, Cyran, Cohn, and Epstein (1993) identified central core phenotype in cardiomyopathy patients' slow skeletal muscle. Many studies since have established subclinical skeletal myopathy, predominantly in slow-twitch muscles, accompanying HCM in animal (Lowey et al., 2018) and human (Cuda et al., 1997; Cuda et al., 1993; Lankford et al., 1995) models. Despite instances of skeletal muscle myopathies with grave outcomes including severe disability, respiratory failure and early death (Månsson, 2014), mutations that cause severe malignant cardiomyopathy – such as in the MYH7 gene – often give only a mild skeletal muscle phenotype (Oldfors, 2007).

Respiratory muscle dysfunction is a prominent feature of heart failure in clinical populations (De Troyer, Borenstein, & Cordier, 1980; Hart et al., 2004; Mancini, Henson, LaManca, & Levine, 1992) and animal models (Howell et al., 1995; Lecarpentier et al., 1999; Stassijns et al., 1998; Supinski, DiMarco, & Dibner-Dunlap, 1994), and dyspnea and reduced exercise capacity are common symptoms in heart failure patients (Gillis et al., 2015). While the etiology of this dysfunction is unclear, it is believed that an increase in eupneic pressure generation imposes an increased workload on the diaphragm and that over time this chronic overworking leads to development of a myopathy. Respiratory muscle in early stage heart failure

has yet to be studied, leaving an important gap in the understanding of the origin of diaphragm dysfunction in this disease. Weakness is additionally reported in peripheral skeletal muscle in heart failure, with important differences from the inspiratory muscle weakness which is more common and more severe (De Sousa et al., 2001; Lindsay et al., 1996), with direct and significant consequences on functional capacity. It serves as an independent prognostic predictor for the disease (Meyer et al., 2001; Ribeiro et al., 2013). Intrinsic dysfunction that develops in the diaphragm has been associated with fiber type shift, atrophy and changes in contractility (Gillis et al., 2015; Lecarpentier et al., 1999; Supinski et al., 1994) as well as changes in intracellular Ca^{2+} regulation (MacFarlane, Darnley, & Smith, 2000) and neurohumoral activation and oxidative stress (Li et al., 2000). The fiber type shift from fast fatigable fibers toward slower fibers with higher oxidative potential appears to be an adaptation to improve endurance capacity of the muscle faced with higher work load. These dysfunctions have been reported under conditions of diastolic as well as systolic impairment (Lavietes, Gerula, Fless, Cherniack, & Arora, 2004; Meyer et al., 2001; Ribeiro, Chiappa, Neder, & Frankenstein, 2009). Supinski et al. (1994) suggest that heart failure can induce myopathic changes, as specific force of diaphragm strips was decreased after experimentally induced heart failure by ventricular pacing in dogs. Gillis et al. (2015) claim that animal models of heart failure, whether induced genetically through hypertrophic or dilated cardiomyopathy or by surgical intervention, show impaired diaphragm function. Gillis et al. (2015) also observed differences in diaphragm myofilament function between heart failure models within each type of intervention. van Hees et al. (2007) examined properties of single diaphragm fibers taken from a rat model of congestive heart failure (CHF) and found reduced maximum force generation, likely due to reduced MHC per half sarcomere as

well as decreased Ca^{2+} sensitivity and slowed crossbridge cycling kinetics (decreased rate constant of force generation and redevelopment).

Despite a common pattern of atrophy, differences in histological changes have been reported between respiratory (diaphragm) and skeletal (limb) muscles. Tikunov, Mancini, and Levine (1996) reported a fast-to-slow shift in myosin and regulatory proteins in diaphragm of patients with CHF, while Drexler et al. (1992) reported a slow-to-fast shift in fibers of limb muscles. This reinforces differences that exist between distal skeletal and respiratory muscles (Lindsay et al., 1996), with one explanation being that the workload of limb muscles tends to decrease in conditions of CHF while that of respiratory muscles increases (Mancini et al., 1992).

Summary

Problem: There is evidence of respiratory dysfunction in conditions of hypertrophic cardiomyopathy, but there have been few studies investigating this topic and its underlying mechanism is unclear. Reasons for such limitation in the literature include difficulty in identifying HCM before it has progressed to heart failure and difficulty in sampling diaphragm of patients. Experimental animal models indirectly show that cardiomyopathy may lead to diaphragm weakness. However, the mechanism behind diaphragm weakness at the cellular level is not clear.

Rationale: The following study investigates diaphragm contractility in a rabbit model of hypertrophic cardiomyopathy using the R403Q mutation. Experiments with permeabilized fibers taken from the diaphragm muscle allow the investigation of the basic contractile unit of muscles – the sarcomere – and therefore eliminate confounding effects of the activation-contraction process and neurogenic factors.

Therefore, the goals of this study are to investigate (i) whether there is weakness at the single fiber level in the diaphragm of transgenic (R403Q) compared with non-transgenic (wild type) conditions, (ii) and whether such weakness is linked to alterations in crossbridge cycling kinetics, as well as (iii) whether such weakness is linked to alterations in calcium sensitivity of the contractile apparatus.

Our hypotheses are:

a) Diaphragm from transgenic (R403Q) rabbit will produce less force than the non-transgenic wild type rabbit;

b) Reduction in force will be due to altered crossbridge kinetics in the transgenic (R403Q) rabbit compared with the nontransgenic wild type rabbit;

c) Reduction in force will be due to alteration in the calcium sensitivity in the transgenic (R403Q) rabbit compared with the nontransgenic wild type rabbit.

CHAPTER II:
EXPERIMENTAL ARTICLE

Abstract

Rationale: There is evidence of respiratory dysfunction and diaphragm weakness in hypertrophic cardiomyopathy. However little is known about the mechanism that underlies this weakness at the muscle fiber level.

Objectives: (i) To test if diaphragm weakness is present in a rabbit model of hypertrophic cardiomyopathy due to underlying R403Q mutation in the β-myosin heavy chain (MHC) and (ii) to determine whether crossbridge kinetics or calcium sensitivity are responsible for this dysfunction.

Hypothesis: Our hypothesis is that the R403Q mutation in β-MHC is responsible for diaphragm muscle weakness caused by abnormal actin-myosin cycling kinetics and calcium dysregulation.

Methods: Diaphragm muscle was dissected from rabbit with R403Q mutation and age-matched control and chemically permeabilized. Individual muscle fibers were isolated and mounted between a force transducer and a length controller, in temperature-controlled chamber. Fibers were submerged in maximal (pCa 4.5) and submaximal (pCa 4.7, 5.0, 5.2, 5.5, 5.7, 6.2, 6.5) activating solutions to elicit isometric contractions followed by a shortening-stretch protocol to measure rate of force redevelopment, a putative measurement of crossbridge kinetics.

Results: Maximum isometric force of R403Q fibers (58.1 ± 11.5 mN/mm^2) was only 61.3% that of WT fibers (94.8 ± 14.2 mN/mm^2). The rate of force redevelopment of R403Q fibers (k_{tr} = 3.31 ± 0.76 s^{-1}) was not significantly different from WT fibers (k_{tr} = 1.89 ± 0.28 s^{-1}) (p=0.15). Calcium sensitivity, measured as pCa_{50} and Hill's slope of force plotted over pCa, was not different between R403Q (pCa_{50} 4.39 ± 0.87, Hill's slope 5.15 ± 2.51) and WT (pCa_{50} 4.98 ± 0.35, Hill's slope 2.74 ± 0.66) fibers (p=0.22 and p=0.97 respectively).

Conclusions: Diaphragm fibers taken from rabbit with R403Q mutation exhibit weakness, but crossbridge kinetics and calcium sensitivity are not responsible for such dysfunction.

INTRODUCTION

Hypertrophic cardiomyopathy (HCM) is the most common genetic cardiac disease affecting an estimated 1 in 500 people (Maron et al., 1995), and the leading cause of sudden death in young athletes (Ho, 2010). The disease is an autosomal dominant inherited trait resulting from the mutation of one or more proteins in the cardiac sarcomere (Greaves et al., 1987; Ho, 2010). Its defining clinical characteristic is hypertrophy of the left ventricle, with evidence of myocyte disarray and interstitial fibrosis at the tissue level (Ho, 2010). There is great variety in the clinical presentation of the disease; some mutation carriers do not exhibit any overt symptoms over their lifetime while others display severe HCM, progressing to end stage heart failure or sudden cardiac death (Michels, Olivotto, Asselbergs, & van der Velden, 2017; Olivotto, Cecchi, Poggesi, & Yacoub, 2012; Velden & Stienen, 2019).

The most common and debilitating symptom of HCM is shortness of breath, particularly during exertion, which is present in up to 90% of patients (Ho, 2010). In fact, respiratory dysfunction has previously been observed in clinical studies of patients with cardiomyopathy (DePaso, Winterbauer, Lusk, Dreis, & Springmeyer, 1991; Fatkin et al., 2000; Ho, 2010; Topol, Traill, & Fortuin, 1985; Witt et al., 1997) and hypertrophic heart failure (Arena et al., 2016; Hughes et al., 1999; Meyer et al., 2001; Ribeiro et al., 2009). Additionally, there is evidence that HCM is accompanied by skeletal myopathy due to the homologous protein mutations in the skeletal muscle sarcomeres (Caforio et al., 1989; Cuda et al., 1997; Cuda et al., 1993; Lowey et al., 2018; Malinchik, Cuda, Podolsky, & Horowits, 1997). Consequently, it is likely that respiratory weakness is caused, at least partially, by alterations in the contractile characteristics of the diaphragm.

Diaphragm weakness has been observed and characterized in studies using animal models of cardiomyopathy and heart failure (De Sousa et al., 2001; Lecarpentier et al., 1998; Lecarpentier et al., 1999; Lecarpentier et al., 1993; Stassijns et al., 1999; van Hees et al., 2007). One of these studies (Lecarpentier et al., 1999), suggested that diaphragm weakness is caused by a decreased myofilament affinity for Ca^{2+}, and ultimately the sensitivity of the contractile apparatus to respond to muscle activation. Other studies suggested that such decrease in Ca^{2+} sensitivity may underlie an impaired muscle relaxation (Sys, Housmans, Van Ocken, & Brutsaert, 1984), and most importantly a decrease in the number of myosin cross-bridges interacting with actin, as well as a decrease in the myosin cross bridge force. In all these cases, the force produced by the diaphragm would be reduced as a result of HCM. Unfortunately, there have not been studies looking at the cellular mechanisms behind diaphragm weakness in HCM, which represents a serious limitation in our understanding of HCM-induced respiratory weakness.

In this study, we used a transgenic rabbit with a missense mutation Arg→Glu at position 403 in the myosin heavy chain (MYH7) gene encoding the β-MHC. This animal model with the R403Q mutation shows no symptoms of disease or premature death at the time of sample collection (Lowey et al., 2018), and thus provides an opportunity for the direct study of the primary disease before the development of secondary adaptations and onset of heart failure. It is currently the only fully characterized animal model that has the same cardiac β-MHC as humans, an important feature since mice, commonly used in HCM studies, possess the α-MHC isoform, which differs in a number of kinetic and functional properties (Lowey et al., 2013; Lowey et al., 2018; Lowey et al., 2008; Van Buren et al., 1995). We examined the mechanics of single diaphragm muscle fibers isolated from the transgenic R403Q rabbits and age-matched controls to

elucidate the mechanism underlying weakness present in diaphragm under conditions of HCM. We observed that fibers isolated from R403Q rabbits present a decrease in fiber-specific force, yet without alterations in the Ca^{2+} sensitivity of the contractile apparatus.

METHODS

Preparation of muscle fibers

Diaphragm muscle was dissected from age-matched R403Q and healthy control rabbits and chemically permeabilized according to standard procedure (Campbell & Moss, 2002; Lowey et al., 2018; Minozzo & Rassier, 2010). The muscles were incubated in rigor solution (pH = 7.0) for approximately 4 hours and then transferred to a 50:50 rigor-glycerol solution for 15 hours. The 50:50 rigor-glycerol solution was replaced with a fresh solution consisting of 50:50 rigor-glycerol and a mix of Roche Diagnostics protease inhibitors and subsequently stored in a -20 °C freezer for 7 days.

On the day of the experiment, a muscle strip of approximately $4mm^2$ was dissected from the original diaphragm sample and defrosted in a fresh rigor solution in a fridge for 1 hour. The strip was then transferred to a relaxing solution (solutions described in detail in later section) and an individual fiber was dissected from the muscle strip. The fiber was secured between two t-shaped aluminum clips and transferred to a fresh relaxing solution in a temperature-controlled chamber whereupon it was mounted onto hooks between a force transducer (resonant frequency 1 kHz) (model 403A, Aurora scientific) and length controller (model 312B, Aurora scientific). Fibres were inspected with a digital camera (HVSL 901A) for potential damage and twisting within the clips, conditions that would stop the experiment. Fiber was adjusted to an initial sarcomere length of 2.7μm before mechanical experimentation.

The protocol was approved by the McGill University Animal Care Committee and complied with the guidelines of the Canadian Council on Animal Care.

Solutions

The rigor solution (pH 7) used for sample storage and defrosting was composed of (in mM) 50 Tris, 100 NaCl, 2 KCl, 2 $MgCl_2$, and 10 EGTA. The relaxing solution, which occupied the first bath of the temperature-controlled experimental chambers, was composed of (in mM): 100 KCl, 2 EGTA, 20 imidazole, 4 ATP, and 7 $MgCl_2$. The pre-activating solution, which had reduced Ca^{2+} buffering capacity and was used immediately prior to each activation to minimize delays in diffusion into the fibre, occupied the second bath and consisted of (in mM): 68 KCl, 0.5 EGTA, 20 Imidazole, 14.5 creatine phosphate, 4.83 ATP, 0.00137 $CaCl_2$, 5.41 $MgCl_2$ and 6.5 HDTA (pH 7.0, pCa 9.0).

The activating solutions of pCa 4.5, 4.7, 5.0, 5.2, 5.5, 5.7, 6.2 and 6.5 were initially selected based on previous work performed in our laboratory (Minozzo & Rassier, 2010). All experimental solutions contained of (in mM): 20 imidazole, 14.5 creatine phosphate, 7 EGTA, 4 MgATP, 1 free Mg^{2+}, free Ca^{2+} ranging from 1nM (pCa 9.0) to 32 μM (pCa 4.5) and KCl to adjust the ionic strength to 180mM. The final concentrations of each metal-ligand complex were calculated with a computer program (Fabiato, 1988).

Stock solutions were prepared in advance from which solutions with active ingredients were prepared in individual quantities of 15ml and subsequently frozen. Each week a set of solutions was thawed for use.

Experimental Setup

The experimental setup, shown in figure 11, consisted of an inverted microscope (Nikon Eclipse TE2000-E, magnification lenses 2x, 10x, 20x) containing a tray onto which the force

transducer, length controller and bath system were mounted (802B, Aurora Scientific). The system was composed of a bath controller (model 802B, Aurora Scientific) and a temperature controller (AD590 temperature sensor that provides a feedback signal to a thermoelectric cooler (TEC) controller, Aurora Scientific). Two camera systems were connected to the microscope, leading to the QCapture and HVSL901 softwares respectively. Force was recorded in volts and converted into mN to appear directly in the ASI600 software during experimental procedure. Images and video footage of the single fiber mounted in experimental setup were recorded using HVSL901A software, and the sarcomere length was subsequently determined using fourier transform analysis in ASI600 software during experimental procedure. Figure 12 shows a mounted fiber at magnifications 2x, 10x, 20x.

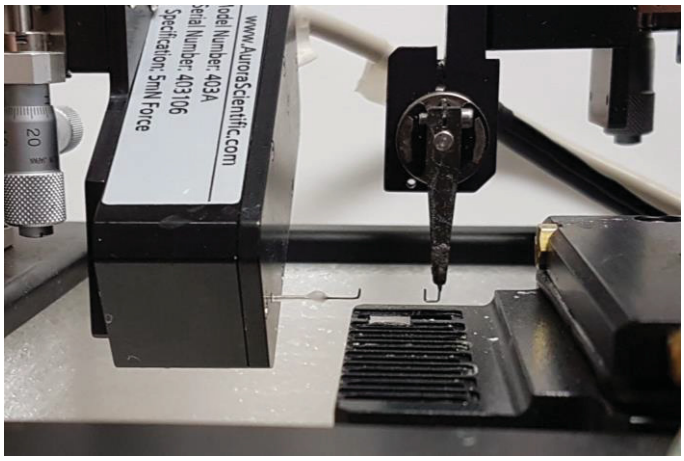

Figure 11: Side view of experimental setup: force transducer, length controller, temperature controlled bath system. Hooks via which aluminum t-clips are mounted on force transducer (left) and length controller (right) are clearly visible

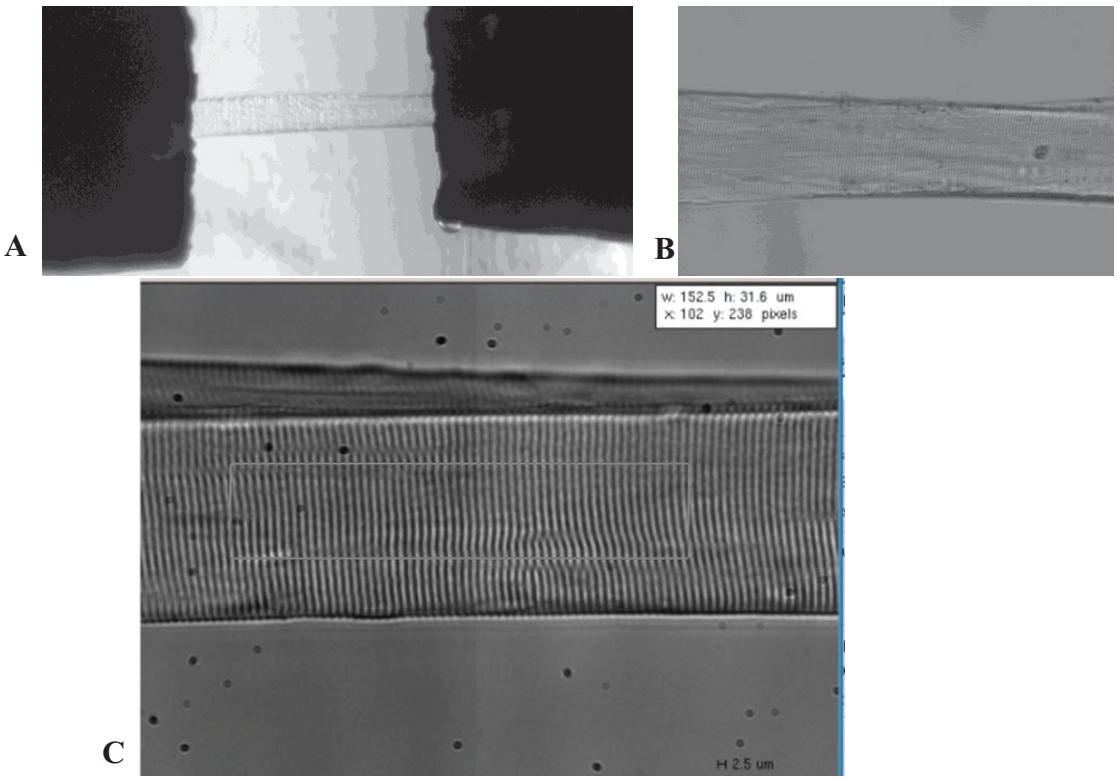

Figure 12: Permeabilized diaphragm muscle fibers mounted in the experimental system at varying magnifications (*A*) 2x magnification, with clips visible. (*B*) 10x magnification, striations are noticeable. (*C*) 20x magnification in HVSL 901A program, striations are distinct and 2.5μm measure is given for scale in bottom right hand corner.

Experimental Protocol

Once secured between the force transducer and length controller, and mounted in the inverted microscope, each fiber was investigated for visible damage and twists/bends - both of which were exclusion criteria for these experiments. The sarcomere length was measured by a high speed video system (HVSL 901A, Aurora Scientific) that used fast fourier transform (FFT) analysis on the average spacing between alternating light (actin) and dark (myosin) bands in a given region of interest. The initial (resting) sarcomere length was set to 2.7μm and the fiber length and diameter (averaged from 3 measurements across its length) were measured and the cross-sectional area was estimated from the diameter assuming circular symmetry. All experiments were conducted at 10°C.

The fiber was subjected to an isometric contraction followed by a shortening-stretch protocol, conducted at each pCa used in the study. Each experiment began with the fiber in relaxing solution (bath 1), followed by a transfer to the pre-activating solution (bath 2) for 5s, and subsequent transfer to the activating solution (baths 3-7) for 35s, followed by a return to the relaxing solution. The order of activating solutions for each fiber started with pCa 4.5, and then was randomized for the subsequent 4 submaximal activating solutions (pCa range = 4.7, 5.0, 5.2, 5.5, 5.7, 6.2, 6.5). A final contraction was again conducted in activating solution pCa 4.5 to check for a potential loss of force during the protocol. During activation of the fibers, after 25s in the experimental solution, a shortening-stretch protocol was conducted (-15% L_o over 15ms, then re-stretch back to L_o over 0.3ms) and the fibre was kept in the activating solution for an additional 10s as force redevelopment occurred. The length of time selected for activation (25s) was found to be sufficient for reaching force of activation plateau during pilot testing while also reducing the total length of time the fibre was kept in activating solution, reducing the possibility for it to become damaged with each contraction.

Data Analysis and Statistics

Maximum isometric force: Experimental force traces were normalized by the fibers' cross-sectional area for each fiber. The maximum isometric contraction force was obtained by subtracting initial force, measured as lowest force produced by the fibre upon submersion in activating solution, from the final force at plateau. This was performed for all fibres at all pCa solutions.

Sarcomere Length Analysis: Initial and final sarcomere length values that corresponded to the same times as the initial and final forces obtained for the maximum isometric force analysis were recorded directly during the experiments.

Rate of force redevelopment (K_{tr}): To calculate the rate of force redevelopment, the force trace was plotted from the lowest value following shortening-stretch sequence to maximum force value measured in plateau just before bath change. The trace was fit with a nonlinear one-phase association by least squares fit:

$$Y = Yo + (Plateau - Yo) * (1 - e^{-kx})$$

where x is time in s and Y is the relative force recorded in mN/mm^2, Yo is the Y value at X_0, Plateau is the Y value at X_∞, and k is the rate constant (in 1/x units).

The fitted value was evaluated with the Residual Sum of Squares (RSS) method:

$$RSS = \sum_i^N (Y_i - \hat{Y}_i)^2$$

$$= \sum_i^N (Y_i - \hat{Y}_0 - (\hat{Y}_\infty - \hat{Y}_0) * (1 - e^{-kx}))^2$$

where Y_i is the observed outcome measure and $\hat{Y}_i$ is the predicted outcome measure according to the model. The RSS is therefore the difference between these two and is minimized iteratively in the least square method to estimate the regression coefficient.

Calcium sensitivity: The isometric contraction forces measured for each fibre were plotted as a function of pCa. A Hill equation was fitted to the data and the pCa_{50} and hill coefficient values for each individual fibre were obtained:

$$\frac{P}{Po} = \frac{1}{1 + 10^h * (pCa_{50} - pCa)}$$

where P is the observed force, P_o is the maximum force (observed for a given fiber at pCa 4.5), h is the hill coefficient, pCa is the $-\log_{(10)}[Ca^{2+}]$, pCa_{50} is the pCa when the force is equal to $P_o/2$ (Walker, Li & Buttrick (2010).

Statistics

All comparisons were performed using Mann-Whitney nonparametric test to account for non-normal distribution of values.

RESULTS

Muscle fibers and descriptive statistics

The muscle fibers used for experimentation had a consistent length for both groups. The variation in the diameter of the R403Q (TG+) samples was approximately twice the size of the wild type (NTG) samples, but still only ~1% of the mean diameter. Fibers were excluded from analysis if they were visibly damaged. The sample sizes were n = 11 and n = 12 for NTG and TG+ muscle respectively. Table 1 provides a summary of the descriptive data for these groups.

Table 1. Sample size and dimensions of fibers from transgenic (TG+) and non-transgenic (NTG) experimental groups

	N	Diameter (mm)*	Length (mm)*
TG+	12	0.113 ± 0.013	1.33 ± 0.129
NTG	11	0.093 ± 0.005	1.32 ± 0.115

*(Mean ± SEM)

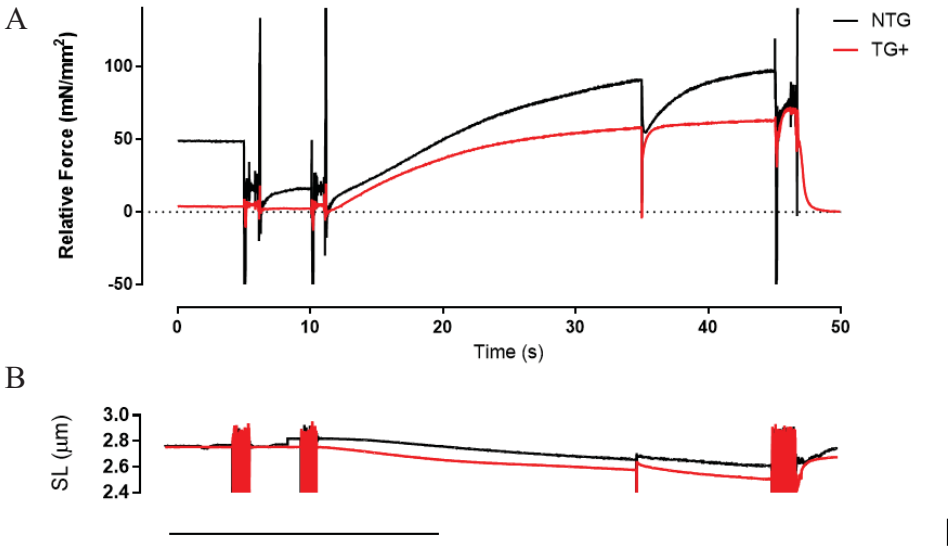

Figure 13: Typical force trace and sarcomere length recordings for isometric contraction followed by shortening-restretch protocol. (*A*) Typical experiment force traces for NTG (black) and TG+ (red) fibers during maximal activation in activating solution pCa 4.5 (*B*) Sarcomere length (SL) changes for each fiber respectively during experiment.

Figure 13a shows the force traces recorded during an experiment with typical fibers from TG+ and NTG groups. In the experimental protocol, the fiber began at rest in relaxing solution (pCa 9.0), was transferred into a pre-activating solution containing ATP and Ca^{2+} buffer and then to an activating solution (in this figure pCa 4.5). The fiber was allowed to contract isometrically and once maximum steady-state force output had been achieved, a shortening-re-stretch protocol was performed, mechanically detaching all crossbridges in a strongly-bound state and allowing the maximum rate of crossbridge cycling (k_{tr}) to be measured during force redevelopment. Figure 13b shows the concurrent change in sarcomere length during the experimental protocol in those same fibers. While the total length of the fiber did not change during the isometric portion of the protocol, there was still some internal shortening and sarcomere non-uniformity that developed within the fiber. The length traces in figure 13b represent one region of the fiber that was monitored over the course of the experimental protocol.

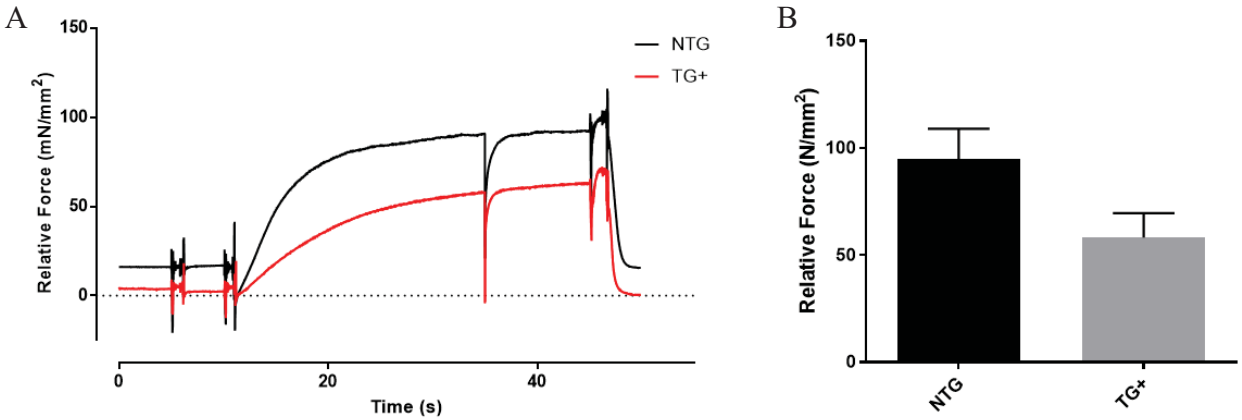

Figure 14: (*A*) Typical force traces during maximal activation (pCa 4.5) for TG+ (red) vs NTG (black) fibers. (*B*) Mean ± SEM force produced during steady-state maximal isometric contraction.

Maximum Isometric Contraction

Figure 14a shows typical force traces for TG+ and NTG fibers maximally activated in solution with pCa 4.5 recorded during a different experiment. Figure 14b shows the corresponding mean values for the two groups. The TG+ fiber group produced lower relative force during maximal isometric contraction (p=0.08). Although statistical significance is usually set for p-values of 0.05 less, we consider here p = 0.08 as significantly different. Given our sample size and the nature of the experiments conducted, declaring these results as nonsignificant would be arbitrary and would not reflect the nature of these experiments that present a considerable variation (Altman, 1990). The mean forces produced by the TG+ and NTG fibers were 58.1 ± 11.5 mN/mm^2 and 94.8 ± 14.2 mN/mm^2 respectively, indicating that the TG+ fibers only produced 61.3% of the force of the NTG fibers.

Rate of Force Redevelopment

Figure 15a shows a zoomed image of typical force traces for TG+ and NTG fibers during the shortening-restretch protocol. The exponential rate of force redevelopment following re-stretch can be clearly seen. Figure 15b shows force traces of the relative rates of redevelopment, where the force for each group is shown as a fraction of its maximum steady state force following restretch. Figure 15c shows the mean k_{tr} values, derived from fitting a first order exponential equation to the redeveloping force trace.

Following the shortening-restretch protocol performed at plateau of maximum isometric contraction (pCa 4.5), TG+ fibers showed a quicker rate of force redevelopment than NTG fibers. However, the values were not statistically different. The mean k_{tr} value obtained for TG+

fibers was 3.31± 0.76 (s^{-1}), 1.75-fold greater than NTG fibers with a mean k_{tr} of 1.89 ± 0.28 s^{-1}) (p=0.15).

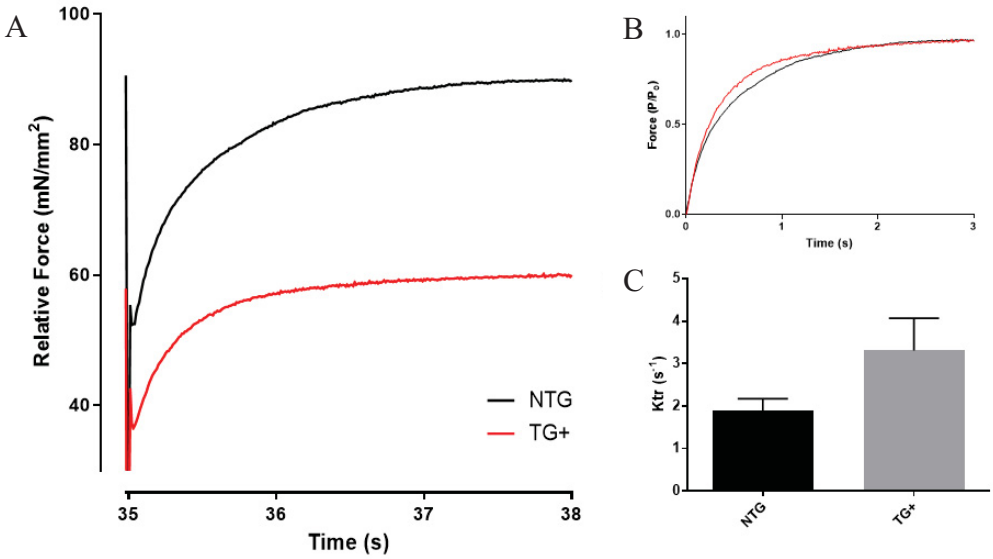

Figure 15: (*A*) Relative force traces during force redevelopment following restretch for TG+ (red) and NTG (black). (*B*) Force redevelopment traces as a fraction of maximum steady-state force achieved following restretch (P/P_o). (*C*) Mean k_{tr} values ± SEM obtained for each group.

Calcium sensitivity

Figure 16 shows force traces for fibers from each experimental group activated at maximal and submaximal Ca^{2+} concentrations. Figures 17a and 17b show an NTG fiber activated at pCa 4.5 and 5.7, while figure 16c shows the sigmoidal Ca^{2+} sensitivity curve derived from the maximum steady state force achieved from activating this fiber at all submaximal Ca^{2+} concentrations tested in this particular experiment (pCa 6.5, 6.2, 5.5). Figures 17d and 17e show a TG+ fiber activated at maximal (pCa 4.5) and submaximal (pCa 5.7) Ca^{2+} concentrations, respectively, while figure 16f shows the Ca^{2+} sensitivity curve calculated using the same method as figure 16c. In figure 16e there is no typical exponential rise in force during redevelopment following shortening-restretch; for many of the TG+ fibers – which exhibited weaker

contractions – at low pCa activation solutions the recoil force of the fiber restretch overpowered the force of contraction.

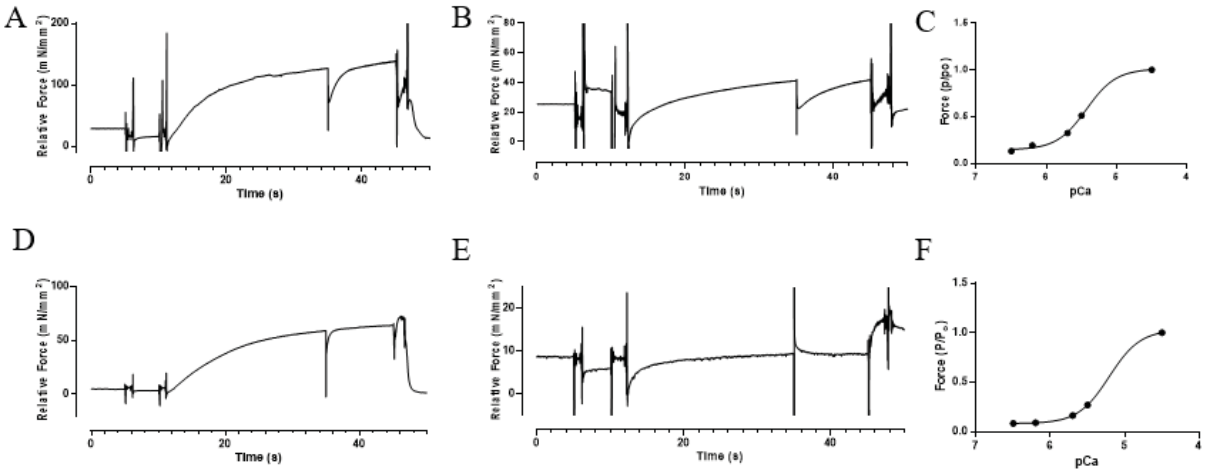

Figure 16: Force traces for active plots (isometric contraction followed by shortening and restretch) of NTG (A, B) and TG+ (D, E) fiber at maximal (pCa 4.5) and submaximal (pCa 5.7) contraction. Relative force for each pCa is plotted as a fraction of maximum force achieved during contraction at pCa 4.5 for each fiber and fitted by a sigmoid curve (C, F). (*A*) NTG fiber activated at pCa 4.5. (*B*) NTG fiber activated at pCa 5.7. (*C*) NTG fiber force-pCa curve. (*D*) TG+ fiber activated at pCa 4.5. (*E*) TG+ fiber activated at pCa 5.7. Recoil following restretch at low forces is seen for TG+ submaximal contraction. (*F*) TG+ fiber force-pCa curve.

Isometric contraction forces for both TG+ and NTG fibers were sensitive to differences in Ca^{2+} concentration in activating solution. In both groups, when fibers forces were plotted as relative force (mN/mm^2) as a function of pCa, they showed the characteristic sigmoid curve fit. There was no difference between the two indices of Ca^{2+} sensitivity of the TG+ and NTG fibers: the mean pCa_{50} was 4.39 ± 0.87 for TG+ compared to 4.98 ± 0.35 for NTG ($p = 0.22$), while the hill coefficient of TG+ was 5.15 ± 2.51 compared to 2.74 ± .066 for NTG ($p = 0.97$). This is clear upon visual inspection of the overlain plots in figure 17a. It is worth noting that the variance in the Hill coefficient, and pCa_{50} to a lesser degree, is much greater in the TG+ than NTG.

Figure 17a shows the curves derived from the average relative force as a function of the mean maximum steady-state force (P/P_o) for each experimental group. Figure 17b shows the mean pCa_{50} for NTG and TG+ groups while 18c shows the mean hill coefficient for NTG and TG+ groups. They were not statistically different (p = 0.22 and 0.97 respectively).

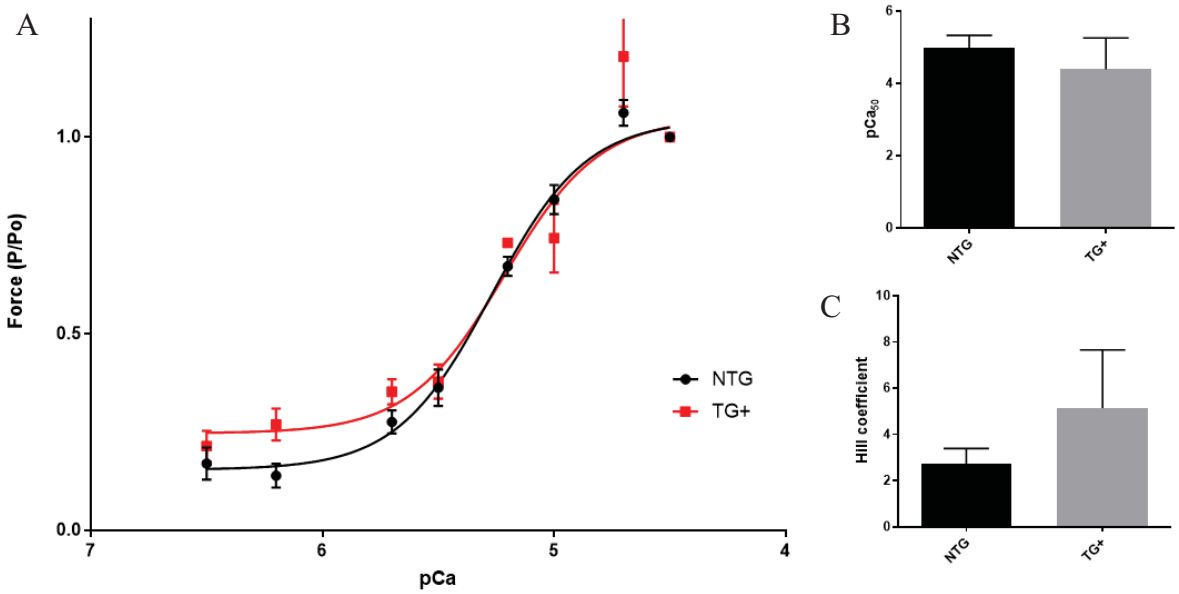

Figure 17: (*A*) Shows relative force values for TG+ and NTG plotted over pCa. (*B*) shows pCa_{50} for TG+ and NTG fibers. (*C*) shows Hill's coefficient for TG+ and NTG fibers.

DISCUSSION

In this study we observed that diaphragm muscle fibers dissected from a transgenic rabbit with the R403Q mutation, that leads to hypertrophic cardiomyopathy, displayed altered contractile function. The TG+ fibers produced less force than the NTG fibers during maximal isometric contraction. However, they showed no difference in either crossbridge kinetics, measured by the rate of force redevelopment following a shortening-restretch protocol, or calcium sensitivity, measured by the pCa_{50} and Hill coefficient, compared with NTG fibers.

There is little research that has been conducted directly with the diaphragm in hypertrophic cardiomyopathy, and its mechanism of dysfunction is unclear. There are several studies performed on patients, but mechanistic interpretation of results is challenging due to the number of confounding variables that can underly muscular dysfunction resulting from the genetic mutation. Background genes and epigenetics, environment, lifestyle or other yet to be identified confounding variables (Fatkin et al., 2000; Ho, 2010; Seidman & Seidman, 2014) can cause considerable variation in the pathophysiology that develops for a given mutation. Family members with the same inherited causal mutation can show very different disease courses, underscoring the disconnect between genotype and clinical outcomes (Ho, 2010). Kirschner et al. (2005) suggest there might even be variation in expression of mutated and wild type protein between cells within a given individual.

Our finding of weakness in the TG+ muscle is consistent with findings of studies looking onto cardiac and other skeletal muscles. Lowey et al. (2018) found a statistically significant reduction in isometric force in R403Q cardiac myofibrils compared with NTG myofibrils, as well as in skeletal (soleus) myofibrils in their study of HCM transgenic rabbit. Malinchik et al. (1997) found a decrease (18%) in isometric tension of type I fibers from soleus muscle taken

from patients with HCM (with identified R403Q mutation) compared to healthy controls. Thus, the diaphragm muscle appears to be affected by the R403Q mutation in a similar manner to both cardiac and other skeletal muscles, producing less force at maximum activation than a healthy control. This weakness is intrinsic to the muscle fiber, independent of atrophy and other cellular disease adaptations.

Diaphragm function has been more thoroughly examined in heart failure patients and experimental models. Hughes et al. (1999) found reduced diaphragm strength in heart failure patients and suggested that skeletal wasting (cardiac cachexia) combined with increased respiratory workload may be contributing to dyspnea in patients, which correlated poorly with left ventricular dysfunction. Meyer et al. (2001) found that inspiratory muscle weakness present in CHF patients was an independent predictor of prognosis. Lecarpentier et al. (1999) also found decreased contractility in diaphragm of rabbits with experimentally induced heart failure. Arena et al. (2016) cited HCM as one type of left side heart disease that causes pulmonary hypertension and respiratory muscle weakness that results in the onset of respiratory muscle fatigue and dyspnea during aerobic exertion.

We failed to observe changes in the rate of force redevelopment (k_{tr}) following restretch in TG+ fibers. The rate of force redevelopment is a putative measure of crossbridge kinetics, with the shortening-restretch protocol detaching (most of) the myosin crossbridges attached in a strongly bound state and allowing their re-attachment to be measured without the confounding effects of calcium-activation mechanism, such as occurs during fiber activation and force development (Brenner & Eisenberg, 1986). This rate, a single order exponential that is supported by a rate constant of similar magnitude in a Huxley-type model, has been correlated with the rate limiting step in the myosin ATPase cycle (Stein et al., 1984). Our results suggest that this rate of

attachment and detachment – the cycling kinetics – of crossbridges is not significantly affected by the R403Q mutation in diaphragm muscle. This result is different from results obtained with cardiac and soleus myofibrils by Lowey et al. (2018), who observed a slower force redevelopment in R403Q rabbits. Since the rate of force redevelopment is a predictor of cross-bridge kinetics, our results suggest that crossbridge cycling is not significantly affected by the R403Q mutation in diaphragm and is not a prominent contributor to muscle weakness.

Our results showed no difference between the Ca^{2+} sensitivity measures (pCa_{50} and Hill coefficient) for TG+ and NTG fibers. An intact Ca^{2+} sensitivity leads us to believe that the fiber's mechanism of activation, comprising both thin filament regulation and cooperativity of myosin crossbridges, is not significantly affected by the R403Q mutation. This appears to be in line with our finding of preserved crossbridge cycling kinetics, since it has been shown that this measure is sensitive to Ca^{2+} activation (Brenner, 1988; Metzger & Moss, 1990). Ca^{2+} sensitivity measured in our permeabilized cell system does not, however, rule out the possibility of dysfunction in the Ca^{2+} handling process at the level of excitation-contraction coupling or during fiber relaxation. Kirschner et al. (2005) examined the myofilaments of soleus muscle from patients with hypertrophic cardiomyopathy (β-MHC mutations were examined albeit not the R403Q mutation) and found that pCa_{50} and cooperativity (hill coefficient) both exhibited differences in mutated tissue compared with healthy control. Furthermore, it was observed that there was marked variability between individual fibers of the same mutation, conditions that were not apparent in the healthy control condition. This disparity in function was thought to cause imbalances in force generation and potentially be a contributing factor to contractile disfunction in both skeletal and more prominently in myocardial muscle. Our results, despite not being statistically significant, perhaps support this as the TG+ hill coefficient standard error is

3.8 fold larger than NTG (and TG+ mean value is nearly double that of NTG). Nagueh et al. (2004) found reduced Ca^{2+} sensitivity of myofibrillar ATPase activity, in proteins isolated from cardiac tissue of R403Q transgenic rabbit compared with healthy age matched controls. MacFarlane et al. (2000) additionally found altered calcium ($[Ca^{2+}]_i$) regulation in diaphragm muscle of a CHF rabbit model that contributed to weakness.

One shortcoming of our study was that we did not perform fiber-type analysis of our fibers after experimentation. This might have influenced experimental outcomes since fiber types, containing different isoform profiles, have different functional characteristics. ATP hydrolysis rates vary across myosin heavy chain isoforms (Sieck et al., 2013), while troponin C isoforms exhibit different Ca^{2+} binding affinities (Geiger, Cody, & Sieck, 1999).

Our results show weakness at the single fiber level in diaphragm muscle with R403Q mutation that at this time does not appear to be due to impairment in crossbridge cycling kinetics or c Ca^{2+} sensitivity. Other aspects of contraction at the fiber level, as well as the myofibril and protein levels, remain to be investigated to elucidate the mechanism underlying this weakness. Further research into the behavior of the myosin crossbridges offers exciting possibilities, especially since the R403Q mutation itself is embedded in the structure of the globular head of the myosin motor. The force generated per crossbridge and the fraction of total number of myosin heads that are in a strongly-bound force-generating state (steady state) are measures that could influence the total force produced during activation that were not addressed in this study. Studies of the R403Q mutation in limb skeletal muscle, cardiac muscle (due to its 'pump' behavior similar to the diaphragm) as well as diaphragm studies in heart failure offer some insight into the mechanism of diaphragm dysfunction in hypertrophic cardiomyopathy due to R403Q mutation. This is however limited due to important established differences between limb

and respiratory muscles (MacFarlane et al., 2000; Polla et al., 2004), differences between skeletal and cardiac muscle and largely different disease etiology and pathophysiology between these two related but distinct diseases. There is need for further study of the diaphragm, specifically, under conditions of hypertrophic cardiomyopathy (including the R403Q mutation) to elucidate the mechanism underlying diaphragm weakness and identify potential therapeutic targets.

CHAPTER III:
CONCLUSIONS AND FUTURE DIRECTIONS

Conclusion

Diaphragm weakness has been observed in patient and Syrian hamster models of hypertrophic cardiomyopathy. This study is the first to directly assess diaphragm muscle function at the fiber level in a rabbit model of HCM using the R403Q mutation, before the onset of heart failure.

Our results support our initial hypothesis that there is intrinsic weakness at the single fiber level of the diaphragm muscle in an R403Q mutation model of hypertrophic cardiomyopathy. However our results disprove our second and third hypotheses. Preserved rate of force redevelopment suggests that crossbridge cycling kinetics (the rate of attachment and detachment of myosin crossbridges) do not contribute significantly to the mechanism that causes this weakness. Meanwhile, no significant change in the pCa_{50} and hill coefficient appear to indicate that Ca^{2+} sensitivity in the TG+ fibers are not affected by the R403Q mutation in HCM and also do not contribute to its mechanism of dysfunction.

Future studies should continue to investigate crossbridge function at both the cellular and subcellular (myofibril, protein) levels of the diaphragm. The fraction of crossbridges that are in a strongly-bound force-generating state during contraction, measured by fiber stiffness through the slack test, as well as the force being generated by each crossbridge might offer further insight into the mechanism of weakness in this muscle.

REFERENCES

Alpert, N. R., Brosseau, C., Federico, A., Krenz, M., Robbins, J., & Warshaw, D. M. (2002). Molecular mechanics of mouse cardiac myosin isoforms. *American Journal of Physiology, 283*(4), H1446-H1454.

Altman, D. G. (1990). *Practical statistics for medical research*: CRC press.

Arena, R., Lavie, C. J., Borghi-Silva, A., Daugherty, J., Bond, S., Phillips, S. A., & Guazzi, M. (2016). Exercise Training in Group 2 Pulmonary Hypertension: Which Intensity and What Modality. *Progress in Cardiovascular Diseases, 59*(1), 87-94. doi:10.1016/j.pcad.2015.11.005

Bagni, M. A., Cecchi, G., Colomo, F., & Garzella, P. (1992). Are weakly binding bridges present in resting intact muscle fibers? *Biophysical Journal, 63*(5), 1412-1415. doi:10.1016/S0006-3495(92)81718-6

Bárány, M. (1967). ATPase activity of myosin correlated with speed of muscle shortening. *The Journal of general physiology, 50*(6), 197-218. doi:10.1085/jgp.50.6.197

Bartoo, M. L., Popov, V. I., Fearn, L. A., & Pollack, G. H. (1993). Active tension generation in isolated skeletal myofibrils. *Journal of Muscle Research & Cell Motility, 14*(5), 498-510. doi:10.1007/bf00297212

Bates, G., Sigurdardottir, S., Kachmar, L., Zitouni, N. B., Benedetti, A., Petrof, B. J., . . . Lauzon, A.-M. (2013). Molecular, cellular, and muscle strip mechanics of the mdx mouse diaphragm. *American Journal of Physiology-Cell Physiology, 304*(9), C873-C880. doi:10.1152/ajpcell.00220.2012

Bertocchini, F., Ovitt, C. E., Conti, A., Barone, V., Schöler, H. R., Bottinelli, R., . . . Sorrentino, V. (1997). Requirement for the ryanodine receptor type 3 for efficient contraction in

neonatal skeletal muscles. *The EMBO journal, 16*(23), 6956-6963. doi:10.1093/emboj/16.23.6956

Biagini, E., Coccolo, F., Ferlito, M., Perugini, E., Rocchi, G., Bacchi-Reggiani, L., . . . Rapezzi, C. (2005). Dilated-Hypokinetic Evolution of Hypertrophic Cardiomyopathy: Prevalence, Incidence, Risk Factors, and Prognostic Implications in Pediatric and Adult Patients. *Journal of the American College of Cardiology, 46*(8), 1543-1550. doi:10.1016/j.jacc.2005.04.062

Blank, S., Chen, V., & Ianuzzo, C. D. (1988). Biochemical characteristics of mammalian diaphragms. *Respiration Physiology, 74*(1), 115-125. doi:10.1016/0034-5687(88)90145-4

Brenner, B. (1988). Effect of Ca2+ on cross-bridge turnover kinetics in skinned single rabbit psoas fibers: implications for regulation of muscle contraction. *Proceedings of the National Academy of Sciences of the United States of America, 85*(9), 3265-3269.

Brenner, B., & Eisenberg, E. (1986). Rate of force generation in muscle: correlation with actomyosin ATPase activity in solution. *Proceedings of the National Academy of Sciences of the United States of America, 83*(10), 3542-3546.

Brenner, B., Yu, L. C., Greene, L. E., Eisenberg, E., & Schoenberg, M. (1986). Ca2+-sensitive cross-bridge dissociation in the presence of magnesium pyrophosphate in skinned rabbit psoas fibers. *Biophysical Journal, 50*(6), 1101-1108. doi:10.1016/S0006-3495(86)83554-8

Brouwer, W. P., Germans, T., Head, M. C., van der Velden, J., Heymans, M. W., Christiaans, I., . . . van Rossum, A. C. (2012). Multiple myocardial crypts on modified long-axis view are a specific finding in pre-hypertrophic HCM mutation carriers. *European Heart Journal - Cardiovascular Imaging, 13*(4), 292-297. doi:10.1093/ehjci/jes005

Burbach, J., Schlenker, E., & Johnson, J. (1987). Morphometry, histochemistry, and contractility of dystrophic hamster diaphragm. *The American journal of physiology, 253*, R275-284. doi:10.1152/ajpregu.1987.253.2.R275

Caforio, A. L. P., Rossi, B., Risaliti, R., Siciliano, G., Marchetti, A., Angelini, C., . . . Muratorio, A. (1989). Type 1 fiber abnormalities in skeletal muscle of patients with hypertrophic and dilated cardiomyopathy: Evidence of subclinical myogenic myopathy. *Journal of the American College of Cardiology, 14*(6), 1464-1473. doi:10.1016/0735-1097(89)90383-5

Campbell, K. (1997). Rate constant of muscle force redevelopment reflects cooperative activation as well as cross-bridge kinetics. *Biophysical Journal, 72*(1), 254-262. doi:10.1016/S0006-3495(97)78664-8

Campbell, K. S., & Lakie, M. (1998). A cross-bridge mechanism can explain the thixotropic short-range elastic component of relaxed frog skeletal muscle. *The Journal of physiology, 510*(3), 941-962. doi:10.1111/j.1469-7793.1998.941bj.x

Campbell, K. S., & Moss, R. L. (2002). History-Dependent Mechanical Properties of Permeabilized Rat Soleus Muscle Fibers. *Biophysical Journal, 82*(2), 929-943. doi:10.1016/S0006-3495(02)75454-4

Captur, G., Flett, A. S., Jacoby, D. L., & Moon, J. C. (2013). Left ventricular non-compaction: The mitral valve prolapse of the 21st century? *International Journal of Cardiology, 164*(1), 3-6. doi:10.1016/j.ijcard.2012.05.018

Cirino, A. L., & Ho, C. (2014). Hypertrophic cardiomyopathy overview. In *GeneReviews®[Internet]*: University of Washington, Seattle.

Citterio, G., Sironi, S., Piccoli, S., & Agostoni, E. (1983). Slow to fast shift in inspiratory muscle fibers during heat tachypnea. *Journal of Respiratory Physiology, 51*(2), 259-274.

Claflin, D. R., & Faulkner, J. A. (1985). Shortening velocity extrapolated to zero load and unloaded shortening velocity of whole rat skeletal muscle. *The Journal of physiology, 359*, 357-363. doi:10.1113/jphysiol.1985.sp015589

Cooke, R. (1995). The actomyosin engine. *9*(8), 636-642. doi:10.1096/fasebj.9.8.7768355

Crilley, J. G., Boehm, E. A., Blair, E., Rajagopalan, B., Blamire, A. M., Styles, P., . . . Watkins, H. (2003). Hypertrophic cardiomyopathy due to sarcomeric gene mutations is characterized by impaired energy metabolism irrespective of the degree of hypertrophy. *Journal of the American College of Cardiology, 41*(10), 1776-1782. doi:10.1016/S0735-1097(02)03009-7

Cuda, G., Fananapazir, L., Epstein, N., & Sellers, J. (1997). The in vitro motility activity of β-cardiac myosin depends on the nature of the β-myosin heavy chain gene mutation in hypertrophic cardiomyopathy. *Journal of Muscle Research & Cell Motility, 18*(3), 275-283. doi:10.1023/a:1018613907574

Cuda, G., Fananapazir, L., Zhu, W. S., Sellers, J. R., & Epstein, N. D. (1993). Skeletal muscle expression and abnormal function of beta-myosin in hypertrophic cardiomyopathy. *The Journal of Clinical Investigation, 91*(6), 2861-2865. doi:10.1172/JCI116530

De Sousa, E., Veksler, V., Bigard, X., Mateo, P., Serrurier, B., & Ventura-Clapier, R. (2001). Dual Influence of Disease and Increased Load on Diaphragm Muscle in Heart Failure. *Journal of molecular and cellular cardiology, 33*(4), 699-710. doi:10.1006/jmcc.2000.1336

De Troyer, A., Borenstein, S., & Cordier, R. (1980). Analysis of lung volume restriction in patients with respiratory muscle weakness. *Thorax, 35*(8), 603-610. doi:10.1136/thx.35.8.603 %J Thorax

DePaso, W. J., Winterbauer, R. H., Lusk, J. A., Dreis, D. P., & Springmeyer, S. C. (1991). Chronic Dyspnea Unexplained by History, Physical Examination, Chest Roentgenogram, and Spirometry: Analysis of a Seven-year Experience. *Chest, 100*(5), 1293-1299. doi:10.1378/chest.100.5.1293

Dos Remedios, C., & Gilmour, D. (2017). An historical perspective of the discovery of titin filaments. *Biophysical reviews, 9*(3), 179-188. doi:10.1007/s12551-017-0269-3

Drexler, H., Riede, U., Münzel, T., König, H., Funke, E., & Just, H. (1992). Alterations of skeletal muscle in chronic heart failure. *Circulation, 85*(5), 1751-1759.

Ecken, J. v. d., Heissler, S. M., Pathan-Chhatbar, S., Manstein, D. J., & Raunser, S. (2016). Cryo-EM structure of a human cytoplasmic actomyosin complex at near-atomic resolution. *Nature, 534*, 724. doi:10.1038/nature18295

Edman, K. A. (1979). The velocity of unloaded shortening and its relation to sarcomere length and isometric force in vertebrate muscle fibres. *The Journal of physiology, 291*, 143-159.

Edman, K. A. (1988). Double-hyperbolic force-velocity relation in frog muscle fibres. *The Journal of physiology, 404*(1), 301-321. doi:10.1113/jphysiol.1988.sp017291

Edman, K. A., & Reggiani, C. (1984). Redistribution of sarcomere length during isometric contraction of frog muscle fibres and its relation to tension creep. *The Journal of physiology, 351*(1), 169-198. doi:10.1113/jphysiol.1984.sp015240

Edman, K. A., & Reggiani, C. (1987). The sarcomere length-tension relation determined in short segments of intact muscle fibres of the frog. *The Journal of physiology, 385*(1), 709-732. doi:10.1113/jphysiol.1987.sp016516

Edman, K. A. P. (1966). The relation between sarcomere length and active tension in isolated semitendinosus fibres of the frog. *The Journal of physiology, 183*(2), 407-417. doi:10.1113/jphysiol.1966.sp007873

Eisenberg, E., & Hill, T. (1985). Muscle contraction and free energy transduction in biological systems. *Science, 227*(4690), 999-1006. doi:10.1126/science.3156404

Elliott, P. M., Gimeno, J. R., Tomé, M. T., Shah, J., Ward, D., Thaman, R., . . . McKenna, W. J. (2006). Left ventricular outflow tract obstruction and sudden death risk in patients with hypertrophic cardiomyopathy. *European Heart Journal, 27*(16), 1933-1941. doi:10.1093/eurheartj/ehl041

Fabiato, A. (1988). Computer programs for calculating total from specified free or free from specified total ionic concentrations in aqueous solutions containing multiple metals and ligands. In *Methods in Enzymology* (Vol. 157, pp. 378-417): Academic Press.

Fabiato, A., & Fabiato, F. (1975). Effects of magnesium on contractile activation of skinned cardiac cells. *The Journal of physiology, 249*(3), 497-517. doi:10.1113/jphysiol.1975.sp011027

Fananapazir, L., Dalakas, M. C., Cyran, F., Cohn, G., & Epstein, N. D. (1993). Missense mutations in the beta-myosin heavy-chain gene cause central core disease in hypertrophic cardiomyopathy. *Proceedings of the National Academy of Sciences of the United States of America, 90*(9), 3993-3997.

Fatkin, D., McConnell, B. K., Mudd, J. O., Semsarian, C., Moskowitz, I. G. P., Schoen, F. J., . . . Seidman, J. G. (2000). An abnormal Ca2+ response in mutant sarcomere protein–mediated familial hypertrophic cardiomyopathy. *The Journal of Clinical Investigation, 106*(11), 1351-1359. doi:10.1172/JCI11093

Fenn, W. (1923). A quantitative comparison between the energy liberated and the work performed by the isolated sartorius muscle of the frog. *The Journal of physiology, 58*(2-3), 175-203.

Fenn, W. O., & Marsh, B. S. (1935). Muscular force at different speeds of shortening. *85*(3), 277-297. doi:10.1113/jphysiol.1935.sp003318

Finer, J. T., Simmons, R. M., & Spudich, J. A. (1994). Single myosin molecule mechanics: piconewton forces and nanometre steps. *Nature, 368*(6467), 113-119. doi:10.1038/368113a0

Flucher, B. E., & Franzini-Armstrong, C. (1996). Formation of junctions involved in excitation-contraction coupling in skeletal and cardiac muscle. *Proceedings of the National Academy of Sciences, 93*(15), 8101-8106. doi:10.1073/pnas.93.15.8101

Franzini-Armstrong, C. (1970). Studies of the Triad I. Structure of the Junction in Frog Twitch Fibers *The Journal of cell biology, 47*(2), 488-499. doi:10.1083/jcb.47.2.488

Franzini-Armstrong, C., & Jorgensen, A. O. (1994). Structure and Development of E-C Coupling Units in Skeletal Muscle. *Annual Review of Physiology, 56*(1), 509-534. doi:10.1146/annurev.ph.56.030194.002453

Fujii, T., Iwane, A. H., Yanagida, T., & Namba, K. (2010). Direct visualization of secondary structures of F-actin by electron cryomicroscopy. *Nature, 467*, 724. doi:10.1038/nature09372

Fujita, H., Sugiura, S., Momomura, S., Omata, M., Sugi, H., & Sutoh, K. (1997). Characterization of mutant myosins of Dictyostelium discoideum equivalent to human familial hypertrophic cardiomyopathy mutants. Molecular force level of mutant myosins

may have a prognostic implication. *The Journal of Clinical Investigation, 99*(5), 1010-1015. doi:10.1172/JCI119228

Geiger, P. C., Cody, M. J., & Sieck, G. C. (1999). Force-calcium relationship depends on myosin heavy chain and troponin isoforms in rat diaphragm muscle fibers. *Journal of Applied Physiology, 87*(5), 1894-1900. doi:10.1152/jappl.1999.87.5.1894

Geisterfer-Lowrance, A. A., Kass, S., Tanigawa, G., Vosberg, H. P., McKenna, W., Seidman, C. E., & Seidman, J. G. (1990). A molecular basis for familial hypertrophic cardiomyopathy: a beta cardiac myosin heavy chain gene missense mutation. *Cell, 62*(5), 999-1006.

Geisterfer-Lowrance, A. A. T., Christe, M., Conner, D. A., Ingwall, J. S., Schoen, F. J., Seidman, C. E., & Seidman, J. G. (1996). A Mouse Model of Familial Hypertrophic Cardiomyopathy. *Science, 272*(5262), 731-734. doi:10.1126/science.272.5262.731

Germans, T., Wilde, A. A. M., Dijkmans, P. A., Chai, W., Kamp, O., Pinto, Y. M., & van Rossum, A. C. (2006). Structural Abnormalities of the Inferoseptal Left Ventricular Wall Detected by Cardiac Magnetic Resonance Imaging in Carriers of Hypertrophic Cardiomyopathy Mutations. *Journal of the American College of Cardiology, 48*(12), 2518-2523. doi:10.1016/j.jacc.2006.08.036

Gillis, T., Klaiman, J., J Foster, A., Platt, M., Huber, J., Corso, M., & Simpson, J. (2015). Dissecting the role of the myofilament in diaphragm dysfunction during the development of heart failure in mice. *American Journal of Physiology- Heart and Circulatory Physiology, 310*, ajpheart.00773.02015. doi:10.1152/ajpheart.00773.2015

Gordon, A. M., Homsher, E., & Regnier, M. (2000). Regulation of Contraction in Striated Muscle. *Physiological Reviews, 80*(2), 853-924. doi:10.1152/physrev.2000.80.2.853

Gordon, A. M., Huxley, A. F., & Julian, F. J. (1966). The variation in isometric tension with sarcomere length in vertebrate muscle fibres. *he Journal of Physiology, 184*(1), 170-192. doi:doi:10.1113/jphysiol.1966.sp007909

Granzier, H. L., & Wang, K. (1993). Passive tension and stiffness of vertebrate skeletal and insect flight muscles: the contribution of weak cross-bridges and elastic filaments. *Biophysical Journal, 65*(5), 2141-2159. doi:10.1016/S0006-3495(93)81262-1

Greaves, S. C., Roche, A. H., Neutze, J. M., Whitlock, R. M., & Veale, A. M. (1987). Inheritance of hypertrophic cardiomyopathy: a cross sectional and M mode echocardiographic study of 50 families. *British Heart Journal, 58*(3), 259-266. doi:10.1136/hrt.58.3.259

Green, H. J., Plyley, M. J., Smith, D. M., & Kile, J. G. (1989). Extreme endurance training and fiber type adaptation in rat diaphragm. *Journal of Applied Physiology, 66*(4), 1914-1920. doi:10.1152/jappl.1989.66.4.1914

Gregorio, C. C., Trombitás, K., Centner, T., Kolmerer, B., Stier, G., Kunke, K., . . . Labeit, S. (1998). The NH2 terminus of titin spans the Z-disc: its interaction with a novel 19-kD ligand (T-cap) is required for sarcomeric integrity. *The Journal of cell biology, 143*(4), 1013-1027. doi:10.1083/jcb.143.4.1013

Greising, S. M., Gransee, H. M., Mantilla, C. B., & Sieck, G. C. (2012). Systems biology of skeletal muscle: fiber type as an organizing principle. *Wiley interdisciplinary reviews. Systems biology and medicine, 4*(5), 457-473. doi:10.1002/wsbm.1184

Güçlü, A., Happé, C., Eren, S., Korkmaz, I. H., Niessen, H. W. M., Klein, P., . . . van der Velden, J. (2015). Left ventricular outflow tract gradient is associated with reduced

capillary density in hypertrophic cardiomyopathy irrespective of genotype. *European Journal of Clinical Investigation, 45*(12), 1252-1259. doi:10.1111/eci.12544

Harris, K. M., Spirito, P., Maron, M. S., Zenovich, A. G., Formisano, F., Lesser, J. R., . . . Maron, B. J. (2006). Prevalence, Clinical Profile, and Significance of Left Ventricular Remodeling in the End-Stage Phase of Hypertrophic Cardiomyopathy. *Circulation, 114*(3), 216-225. doi:10.1161/CIRCULATIONAHA.105.583500

Hart, N., Kearney, M. T., Pride, N. B., Green, M., Lofaso, F., Shah, A. M., . . . Polkey, M. I. (2004). Inspiratory muscle load and capacity in chronic heart failure. *Thorax, 59*(6), 477-482. doi:10.1136/thx.2003.007724

Hasenfuss, G. (1998). Animal models of human cardiovascular disease, heart failure and hypertrophy. *Cardiovasc Res, 39*(1), 60-76.

Hellam, D. C., & Podolsky, R. J. (1969). Force measurements in skinned muscle fibres. *The Journal of physiology, 200*(3), 807-819. doi:10.1113/jphysiol.1969.sp008723

Herzog, W., Powers, K., Johnston, K., & Duvall, M. (2015). A new paradigm for muscle contraction. *Frontiers in Physiology, 6*(174). doi:10.3389/fphys.2015.00174

Hill, A. V. (1910). The possible effects of the aggregation of the molecules of haemoglobin on its dissociation curves. *The Journal of physiology, 40*, 4-7.

Hill, A. V. (1938). The heat of shortening and the dynamic constants of muscle. *Proceedings of the Royal Society B, 126*(843), 136-195. doi:doi:10.1098/rspb.1938.0050

Hill, D. K. (1968). Tension due to interaction between the sliding filaments in resting striated muscle. the effect of stimulation. *The Journal of physiology, 199*(3), 637-684. doi:10.1113/jphysiol.1968.sp008672

Ho, C. Y. (2010). Hypertrophic cardiomyopathy. *Heart failure clinics, 6*(2), 141-159. doi:10.1016/j.hfc.2009.12.001

Ho, C. Y. (2012). Genetic Considerations in Hypertrophic Cardiomyopathy. *Progress in Cardiovascular Diseases, 54*(6), 456-460. doi:10.1016/j.pcad.2012.03.004

Ho, C. Y. (2016). Integrating genetics and medicine: Disease-modifying treatment strategies for hypertrophic cardiomyopathy. *Progress in Pediatric Cardiology, 40*, 21-23. doi:10.1016/j.ppedcard.2016.01.007

Ho, C. Y., Abbasi, S. A., Neilan, T. G., Shah, R. V., Chen, Y., Heydari, B., . . . Kwong, R. Y. (2013). T1 measurements identify extracellular volume expansion in hypertrophic cardiomyopathy sarcomere mutation carriers with and without left ventricular hypertrophy. *Circulation. Cardiovascular imaging, 6*(3), 415-422. doi:10.1161/CIRCIMAGING.112.000333

Ho, C. Y., & Seidman, C. E. (2006). A Contemporary Approach to Hypertrophic Cardiomyopathy. *Circulation, 113*(24), e858-e862. doi:doi:10.1161/CIRCULATIONAHA.105.591982

Hodge, K., Powers, S. K., Coombes, J., Fletcher, L., Demirel, H. A., Dodd, S. L., & Martin, D. (1997). Bioenergetic characteristics of the costal and crural diaphragm in mammals. *Respiration Physiology, 109*(2), 149-154. doi:10.1016/S0034-5687(97)00051-0

Houdusse, A., & Sweeney, H. L. (2016). How Myosin Generates Force on Actin Filaments. *Trends in Biochemical Sciences, 41*(12), 989-997. doi:10.1016/j.tibs.2016.09.006

Howell, S., Maarek, J. M., Fournier, M., Sullivan, K., Zhan, W. Z., & Sieck, G. C. (1995). Congestive heart failure: differential adaptation of the diaphragm and latissimus dorsi. *Journal of Applied Physiology, 79*(2), 389-397. doi:10.1152/jappl.1995.79.2.389

Hughes, P. D., Polkey, M. I., Harris, M. L., Coats, A. J. S., Moxham, J., & Green, M. (1999). Diaphragm Strength In Chronic Heart Failure. *160*(2), 529-534. doi:10.1164/ajrccm.160.2.9810081

Huxley, A. F., & Niedergerke, R. (1954). Structural Changes in Muscle During Contraction: Interference Microscopy of Living Muscle Fibres. *Nature, 173*(4412), 971-973. doi:10.1038/173971a0

Huxley, A. F., & Simmons, R. M. (1971). Proposed Mechanism of Force Generation in Striated Muscle. *Nature, 233*(5321), 533-538. doi:10.1038/233533a0

Huxley, A. F., & Taylor, R. E. (1958). Local activation of striated muscle fibres. *The Journal of physiology, 144*(3), 426-441. doi:10.1113/jphysiol.1958.sp006111

Huxley, H., & Hanson, J. (1954). Changes in the Cross-Striations of Muscle during Contraction and Stretch and their Structural Interpretation. *Nature, 173*(4412), 973-976. doi:10.1038/173973a0

Huxley, H. E. (1953). Electron microscope studies of the organisation of the filaments in striated muscle. *Biochimica et Biophysica Acta, 12*(1), 387-394. doi:10.1016/0006-3002(53)90156-5

Huxley, H. E. (1957). The double array of filaments in cross-striated muscle. *The Journal of biophysical and biochemical cytology, 3*(5), 631-648.

Huxley, H. E. (1963). Electron microscope studies on the structure of natural and synthetic protein filaments from striated muscle. *Journal of Molecular Biology, 7*(3), 281-IN230. doi:10.1016/S0022-2836(63)80008-X

Huxley, H. E. (1969). The Mechanism of Muscular Contraction. *Science, 164*(3886), 1356-1366. doi:10.1126/science.164.3886.1356

Huxley, H. E. (1973). *Structural Changes in the Actin-and Myosin-eontaining Filaments during Contraction.* Paper presented at the Cold Spring Harbor Symposia on Quantitative Biology.

Huxley, H. E. (2004). Fifty years of muscle and the sliding filament hypothesis. *European Journal of Biochemistry, 271*(8), 1403-1415. doi:doi:10.1111/j.1432-1033.2004.04044.x

Jaenicke, T., Diederich, K. W., Haas, W., Schleich, J., Lichter, P., Pfordt, M., . . . Vosberg, H.-P. (1990). The complete sequence of the human β-myosin heavy chain gene and a comparative analysis of its product. *Genomics, 8*(2), 194-206. doi:10.1016/0888-7543(90)90272-V

Jasmin, G., & Proschek, L. (1982). Hereditary polymyopathy and cardiomyopathy in the syrian hamster. I. Progression of heart and skeletal muscle lesions in the UM-X7.1 line. *Muscle Nerve, 5*(1), 20-25. doi:10.1002/mus.880050105

Julian, F. J., Sollins, K. R., & Sollins, M. R. (1974). A Model for the Transient and Steady-State Mechanical Behavior of Contracting Muscle. *Biophysical Journal, 14*(7), 546-562. doi:10.1016/S0006-3495(74)85934-5

Katzemich, A., Kreisköther, N., Alexandrovich, A., Elliott, C., Schöck, F., Leonard, K., . . . Bullard, B. (2012). The function of the M-line protein obscurin in controlling the symmetry of the sarcomere in the flight muscle of Drosophila. *Journal of cell science, 125*(Pt 14), 3367-3379. doi:10.1242/jcs.097345

Kavinsky, C. J., Umeda, P. K., Levin, J. E., Sinha, A. M., Nigro, J. M., Jakovcic, S., & Rabinowitz, M. (1984). Analysis of cloned mRNA sequences encoding subfragment 2 and part of subfragment 1 of alpha- and beta-myosin heavy chains of rabbit heart. *Journal of Biological Chemistry, 259*(5), 2775-2781.

Kirschner, S. E., Becker, E., Antognozzi, M., Kubis, H.-P., Francino, A., Navarro-López, F., . . . Kraft, T. (2005). Hypertrophic cardiomyopathy-related β-myosin mutations cause highly variable calcium sensitivity with functional imbalances among individual muscle cells. *American Journal of Physiology-Heart and Circulatory Physiology, 288*(3), H1242-H1251. doi:10.1152/ajpheart.00686.2004

Kitamura, K., Tokunaga, M., Iwane, A. H., & Yanagida, T. (1999). A single myosin head moves along an actin filament with regular steps of 5.3 nanometres. *Nature, 397*(6715), 129-134. doi:10.1038/16403

Kreutziger, K. L., Piroddi, N., Scellini, B., Tesi, C., Poggesi, C., & Regnier, M. (2008). Thin filament Ca2+ binding properties and regulatory unit interactions alter kinetics of tension development and relaxation in rabbit skeletal muscle. *The Journal of physiology, 586*(15), 3683-3700. doi:10.1113/jphysiol.2008.152181

Labeit, S., & Kolmerer, B. (1995). Titins: Giant Proteins in Charge of Muscle Ultrastructure and Elasticity. *Science, 270*(5234), 293-296. doi:10.1126/science.270.5234.293

Lakdawala, N. K., Thune, J. J., Maron, B. J., Cirino, A. L., Havndrup, O., Bundgaard, H., . . . Ho, C. Y. (2011). Electrocardiographic Features of Sarcomere Mutation Carriers With and Without Clinically Overt Hypertrophic Cardiomyopathy. *The American Journal of Cardiology, 108*(11), 1606-1613. doi:10.1016/j.amjcard.2011.07.019

Lankford, E., Epstein, N., Fananapazir, L., & Sweeney, H. (1995). Abnormal contractile properties of muscle fibers expressing [beta]-myosin chain mutations in patients with hypertrophic cardiomyopathy. *The Journal of Clinical Investigation, 95*, 1409-1414. doi:10.1172/JCI117795

Lavietes, M. H., Gerula, C. M., Fless, K. G., Cherniack, N. S., & Arora, R. R. (2004). Inspiratory Muscle Weakness in Diastolic Dysfunction. *Chest, 126*(3), 838-844. doi:10.1378/chest.126.3.838

Lecarpentier, Y., Chemla, D., Blanc, F.-X., C Pourny, J., Joseph, T., Riou, B., & Coirault, C. (1998). Mechanics, energetics, and crossbridge kinetics of rabbit diaphragm during congestive heart failure. *The FASEB Journal, 12*, 981-989. doi:10.1096/fasebj.12.11.981

Lecarpentier, Y., Coirault, C., Langeron, O., Blanc, F.-X., Salmeron, S., Attal, P., . . . Chemla, D. (1999). Impaired load dependence of diaphragm relaxation during congestive heart failure in the rabbit. *Journal of Applied Physiology, 87*, 1339-1345. doi:10.1152/jappl.1999.87.4.1339

Lecarpentier, Y., Coirault, C., Lerebours, G., Desche, P., Scalbert, E., Lambert, F., & Chemla, D. (1997). Effects of angiotensin converting enzyme inhibition on crossbridge properties of diaphragm in cardiomyopathic hamsters of the dilated bio 53-58 strain. *American journal of respiratory critical care medicine, 155*(2), 630-636.

Lecarpentier, Y., Pery, N., Coirault, C., Scalbert, E., Desche, P., Suard, I., . . . Chemla, D. (1993). Intrinsic alterations of diaphragm muscle in experimental cardiomyopathy. *American Heart Journal, 126*(3, Part 2), 770-776. doi:10.1016/0002-8703(93)90928-3

Lehman, W., Craig, R., & Vibert, P. (1994). Ca2+-induced tropomyosin movement in Limulus thin filaments revealed by three-dimensional reconstruction. *Nature, 368*(6466), 65-67. doi:10.1038/368065a0

Levine, S., Kaiser, L., Leferovich, J., & Tikunov, B. (1997). Cellular Adaptations in the Diaphragm in Chronic Obstructive Pulmonary Disease. *New England Journal of Medicine, 337*(25), 1799-1806. doi:10.1056/nejm199712183372503

Li, X., Moody, M. R., Engel, D., Walker, S., Clubb Jr, F. J., Sivasubramanian, N., . . . Reid, M. B. (2000). Cardiac-specific overexpression of tumor necrosis factor-α causes oxidative stress and contractile dysfunction in mouse diaphragm. *Circulation, 102*(14), 1690-1696.

Lindsay, D. C., Lovegrove, C. A., Dunn, M. J., Bennett, J. G., Pepper, J. R., Yacoub, M. H., & Poole-Wilson, P. A. (1996). Histological abnormalities of muscle from limb, thorax and diaphragm in chronic heart failure. *European Heart Journal, 17*(8), 1239-1250. doi:10.1093/oxfordjournals.eurheartj.a015042

Littlefield, R. S., & Fowler, V. M. (2008). Thin filament length regulation in striated muscle sarcomeres: Pointed-end dynamics go beyond a nebulin ruler. *Seminars in Cell & Developmental Biology, 19*(6), 511-519. doi:10.1016/j.semcdb.2008.08.009

Lorenz, M., & Holmes, K. C. (2010). The actin-myosin interface. *Proceedings of the National Academy of Sciences of the United States of America, 107*(28), 12529-12534. doi:10.1073/pnas.1003604107

Lowey, S. (2002). Functional Consequences of Mutations in the Myosin Heavy Chain at Sites Implicated in Familial Hypertrophic Cardiomyopathy. *Trends in cardiovascular medicine, 12*, 348-354. doi:10.1016/S1050-1738(02)00181-0

Lowey, S., Bretton, V., Gulick, J., Robbins, J., & Trybus, K. M. (2013). Transgenic mouse α- and β-cardiac myosins containing the R403Q mutation show isoform-dependent transient kinetic differences. *The Journal of biological chemistry, 288*(21), 14780-14787. doi:10.1074/jbc.M113.450668

Lowey, S., Bretton, V., Joel, P. B., Trybus, K. M., Gulick, J., Robbins, J., . . . Rassier, D. E. (2018). Hypertrophic cardiomyopathy R403Q mutation in rabbit β-myosin reduces

contractile function at the molecular and myofibrillar levels. *Proceedings of the National Academy of Sciences, 115*(44), 11238-11243. doi:10.1073/pnas.1802967115

Lowey, S., Lesko, L. M., Rovner, A. S., Hodges, A. R., White, S. L., Low, R. B., . . . Robbins, J. (2008). Functional Effects of the Hypertrophic Cardiomyopathy R403Q Mutation Are Different in an α- or β-Myosin Heavy Chain Backbone. *Journal of Biological Chemistry, 283*(29), 20579-20589. doi:10.1074/jbc.M800554200

MacFarlane, N. G., Darnley, G. M., & Smith, G. L. (2000). Cellular basis for contractile dysfunction in the diaphragm from a rabbit infarct model of heart failure. *American Journal of Physiology-Cell Physiology, 278*(4), C739-C746. doi:10.1152/ajpcell.2000.278.4.C739

Malinchik, S., Cuda, G., Podolsky, R. J., & Horowits, R. (1997). Isometric Tension and Mutant Myosin Heavy Chain Content in Single Skeletal Myofibers from Hypertrophic Cardiomyopathy Patients. *Journal of molecular and cellular cardiology, 29*(2), 667-676. doi:10.1006/jmcc.1996.0309

Malmqvist, U., Aronshtam, A., & Lowey, S. (2004). Cardiac Myosin Isoforms from Different Species Have Unique Enzymatic and Mechanical Properties. *Biochemistry, 43*, 15058-15065. doi:10.1021/bi0495329

Mancini, D. M., Henson, D., LaManca, J., & Levine, S. (1992). Respiratory muscle function and dyspnea in patients with chronic congestive heart failure. *Circulation, 86*(3), 909-918.

Månsson, A. (2014). Hypothesis and theory: mechanical instabilities and non-uniformities in hereditary sarcomere myopathies. *Frontiers in Physiology, 5*(350). doi:10.3389/fphys.2014.00350

Marian, A. J., & Braunwald, E. (2017). Hypertrophic Cardiomyopathy. *Circulation research, 121*(7), 749-770. doi:10.1161/CIRCRESAHA.117.311059

Marian, A. J., Wu, Y., Lim, D. S., McCluggage, M., Youker, K., Yu, Q. T., . . . Roberts, R. (1999). A transgenic rabbit model for human hypertrophic cardiomyopathy. *The Journal of Clinical Investigation, 104*(12), 1683-1692. doi:10.1172/JCI7956

Marin-Garcia, J. (2007). CHAPTER 13 - Cardiomyopathies. In J. Marin-Garcia (Ed.), *Post-Genomic Cardiology* (pp. 363-413). Burlington: Academic Press.

Maron, B. J., Gardin, J. M., Flack, J. M., Gidding, S. S., Kurosaki, T. T., & Bild, D. E. (1995). Prevalence of Hypertrophic Cardiomyopathy in a General Population of Young Adults. *Circulation, 92*(4), 785-789. doi:10.1161/01.CIR.92.4.785

Maron, B. J., Maron, M. S., & Semsarian, C. (2012). Genetics of hypertrophic cardiomyopathy after 20 years: clinical perspectives. *Journal of Cardiovascular Translational Research, 60*(8), 705-715.

Maron, B. J., McKenna, W. J., Danielson, G. K., Kappenberger, L. J., Kuhn, H. J., Seidman, C. E., . . . Torbicki, A. (2003). American College of Cardiology/European Society of Cardiology Clinical Expert Consensus Document on Hypertrophic Cardiomyopathy: a report of the American College of Cardiology Foundation Task Force on Clinical Expert Consensus Documents and the European Society of Cardiology Committee for Practice Guidelines. *Journal of the American College of Cardiology, 42*(9), 1687-1713. doi:10.1016/S0735-1097(03)00941-0

Maron, B. J., Olivotto, I., Spirito, P., Casey, S. A., Bellone, P., Gohman, T. E., . . . Cecchi, F. (2000). Epidemiology of Hypertrophic Cardiomyopathy. *Circulation, 102*(8), 858-864. doi:10.1161/01.CIR.102.8.858

Maron, M. S., Olivotto, I., Betocchi, S., Casey, S. A., Lesser, J. R., Losi, M. A., . . . Maron, B. J. (2003). Effect of Left Ventricular Outflow Tract Obstruction on Clinical Outcome in Hypertrophic Cardiomyopathy. *New England Journal of Medicine, 348*(4), 295-303. doi:10.1056/NEJMoa021332

Maron, M. S., Olivotto, I., Zenovich, A. G., Link, M. S., Pandian, N. G., Kuvin, J. T., . . . Maron, B. J. (2006). Hypertrophic Cardiomyopathy Is Predominantly a Disease of Left Ventricular Outflow Tract Obstruction. *Circulation, 114*(21), 2232-2239. doi:10.1161/CIRCULATIONAHA.106.644682

Masataka, & Halvorson. (2008). Force transients and minimum cross-bridge models in muscular contraction. *Journal of Muscle Research - Cell Motility, 28*(7), 371. doi:10.1007/s10974-008-9131-3

McNally, E. M., Kraft, R., Bravo-Zehnder, M., Taylor, D. A., & Leinwand, L. A. J. J. o. m. b. (1989). Full-length rat alpha and beta cardiac myosin heavy chain sequences: comparisons suggest a molecular basis for functional differences. *Journal of Molecular Biology, 210*(3), 665-671.

Metzger, J., & Moss, R. (1990). Calcium-sensitive cross-bridge transitions in mammalian fast and slow skeletal muscle fibers. *Science, 247*(4946), 1088-1090. doi:10.1126/science.2309121

Meyer, F., Borst, M., Zugck, C., Kirschke, A., Schellberg, D., Kübler, W., & Haass, M. (2001). Respiratory Muscle Dysfunction in Congestive Heart Failure : Clinical Correlation and Prognostic Significance. *Circulation, 103*, 2153-2158. doi:10.1161/01.CIR.103.17.2153

Michels, M., Olivotto, I., Asselbergs, F. W., & van der Velden, J. (2017). Life-long tailoring of management for patients with hypertrophic cardiomyopathy : Awareness and decision-

making in changing scenarios. *Netherlands heart journal 25*(3), 186-199. doi:10.1007/s12471-016-0943-2

Minozzo, F. C., & Rassier, D. E. (2010). Effects of blebbistatin and Ca2+ concentration on force produced during stretch of skeletal muscle fibers. *American Journal of Physiology-Cell Physiology, 299*(5), C1127-C1135. doi:10.1152/ajpcell.00073.2010

Mintz, B., & Baker, W. W. (1967). Normal mammalian muscle differentiation and gene control of isocitrate dehydrogenase synthesis. *Proceedings of the National Academy of Sciences of the United States of America, 58*(2), 592-598.

Mizuno, M. (1991). Human respiratory muscles: fibre morphology and capillary supply. *European Respiratory Journal, 4*(5), 587-601.

Muthuchamy, M., Pieples, K., Rethinasamy, P., Hoit, B., Grupp, I. L., Boivin, G. P., . . . Wieczorek, D. F. (1999). Mouse Model of a Familial Hypertrophic Cardiomyopathy Mutation in alpha-Tropomyosin Manifests Cardiac Dysfunction. *Circulation research, 85*(1), 47-56. doi:10.1161/01.RES.85.1.47

Mutungi, G. (2003). The effects of inorganic phosphate and arsenate on both passive muscle visco-elasticity and maximum Ca 2+ activated tension in chemically skinned rat fast and slow twitch muscle fibres. *Journal of Muscle Research - Cell Motility, 24*(1), 65-75.

Nagueh, S. F., Chen, S., Patel, R., Tsybouleva, N., Lutucuta, S., Kopelen, H. A., . . . Marian, A. J. (2004). Evolution of expression of cardiac phenotypes over a 4-year period in the beta-myosin heavy chain-Q403 transgenic rabbit model of human hypertrophic cardiomyopathy. *Journal of molecular and cellular cardiology, 36*(5), 663-673. doi:10.1016/j.yjmcc.2004.02.010

Oberst, L., Zhao, G., Park, J. T., Brugada, R., Michael, L. H., Entman, M. L., . . . Marian, A. J. (1998). Dominant-negative effect of a mutant cardiac troponin T on cardiac structure and function in transgenic mice. *The Journal of Clinical Investigation, 102*(8), 1498-1505. doi:10.1172/JCI4088

Ohtsuki, I., Masaki, T., Nonomura, Y., & Ebashi, S. (1967). Periodic Distribution of Troponin along the Thin Filament. *The Journal of Biochemistry, 61*(6), 817-819. doi:10.1093/oxfordjournals.jbchem.a128619

Oldfors, A. (2007). Hereditary myosin myopathies. *Neuromuscular Disorders, 17*(5), 355-367. doi:10.1016/j.nmd.2007.02.008

Olivotto, I., Cecchi, F., Poggesi, C., & Yacoub, M. H. (2012). Patterns of Disease Progression in Hypertrophic Cardiomyopathy. *Circulation: Heart Failure, 5*(4), 535-546. doi:10.1161/CIRCHEARTFAILURE.112.967026

OpenStax. (2016). *Anatomy & Physiology*. In OpenStax CNX (Ed.). Retrieved from http://cnx.org/contents/14fb4ad7-39a1-4eee-ab6e-3ef2482e3e22@8.24.

Pagani, E. D., Shemin, R., & Julian, F. J. (1986). Tension-pCa relations of saponin-skinned rabbit and human heart muscle. *Journal of molecular and cellular cardiology, 18*(1), 55-66. doi:10.1016/S0022-2828(86)80982-8

Page, S. G., & Huxley, H. E. (1963). Filament lengths in striated muscle *The Journal of cell biology, 19*(2), 369-390. doi:10.1083/jcb.19.2.369

Palmer, B. M., Suzuki, T., Wang, Y., Barnes, W. D., Miller, M. S., & Maughan, D. W. (2007). Two-state model of acto-myosin attachment-detachment predicts C-process of sinusoidal analysis. *Biophysical Journal, 93*(3), 760-769. doi:10.1529/biophysj.106.101626

Palmiter, K. A., Tyska, M. J., Haeberle, J. R., Alpert, N. R., Fananapazir, L., & Warshaw, D. M. (2000). R403Q and L908V mutant β-cardiac myosin from patients with familial hypertrophic cardiomyopathy exhibit enhanced mechanical performance at the single molecule level. *Journal of Muscle Research - Cell Motility, 21*(7), 609-620. doi:10.1023/a:1005678905119

Periasamy, M., & Kalyanasundaram, A. (2007). SERCA pump isoforms: Their role in calcium transport and disease. *Muscle Nerve, 35*(4), 430-442. doi:10.1002/mus.20745

Polla, B., D'Antona, G., Bottinelli, R., & Reggiani, C. (2004). Respiratory muscle fibres: specialisation and plasticity. *Thorax, 59*(9), 808-817. doi:10.1136/thx.2003.009894

Potma, E. J., van Graas, I. A., & Stienen, G. J. (1995). Influence of inorganic phosphate and pH on ATP utilization in fast and slow skeletal muscle fibers. *Biophysical Journal, 69*(6), 2580-2589. doi:10.1016/S0006-3495(95)80129-3

Prado, L. G., Makarenko, I., Andresen, C., Krüger, M., Opitz, C. A., & Linke, W. A. (2005). Isoform diversity of giant proteins in relation to passive and active contractile properties of rabbit skeletal muscles. *The Journal of general physiology, 126*(5), 461-480. doi:10.1085/jgp.200509364

Proske, U., & Morgan, D. (1999). Do cross-bridges contribute to the tension during stretch of passive muscle? *Journal of Muscle Research and Cell Motility, 20*, 433-442. doi:10.1023/A:1005573625675

Rassier, D. E. (2010). *Muscle Biophysics*: Springer.

Rayment, I., Holden, H., Whittaker, M., Yohn, C., Lorenz, M., Holmes, K., & Milligan, R. (1993). Structure of the actin-myosin complex and its implications for muscle contraction. *Science, 261*(5117), 58-65. doi:10.1126/science.8316858

Rayment, I., Holden, H. M., Sellers, J. R., Fananapazir, L., & Epstein, N. D. (1995). Structural interpretation of the mutations in the beta-cardiac myosin that have been implicated in familial hypertrophic cardiomyopathy. *Proceedings of the National Academy of Sciences of the United States of America, 92*(9), 3864-3868. doi:10.1073/pnas.92.9.3864

Reggiani, C. (2007). When fibres go slack and cross bridges are free to run: a brilliant method to study kinetic properties of acto-myosin interaction. *The Journal of physiology, 583*(Pt 1), 5-7. doi:10.1113/jphysiol.2007.137000

Ribeiro, J. P., Chiappa, G. R., Neder, J. A., & Frankenstein, L. J. C. H. F. R. (2009). Respiratory muscle function and exercise intolerance in heart failure. *Current Heart Failure Reports, 6*(2), 95-101. doi:10.1007/s11897-009-0015-7

Ribeiro, P. A. B., Ribeiro, J. P., Minozzo, F. C., Pavlov, I., Leu, N. A., Kurosaka, S., . . . Rassier, D. E. (2013). Contractility of myofibrils from the heart and diaphragm muscles measured with atomic force cantilevers: Effects of heart-specific deletion of arginyl-tRNA–protein transferase. *International Journal of Cardiology, 168*(4), 3564-3571. doi:10.1016/j.ijcard.2013.05.069

Roche, S. M., Gumucio, J. P., Brooks, S. V., Mendias, C. L., & Claflin, D. R. (2015). Measurement of Maximum Isometric Force Generated by Permeabilized Skeletal Muscle Fibers. *JoVE*(100), e52695. doi:doi:10.3791/52695

Rossi, R., Bottinelli, R., Sorrentino, V., & Reggiani, C. (2001). Response to caffeine and ryanodine receptor isoforms in mouse skeletal muscles. *American Journal of Physiology-Cell Physiology, 281*(2), C585-C594. doi:10.1152/ajpcell.2001.281.2.C585

Ruff, C., Furch, M., Brenner, B., Manstein, D. J., & Meyhöfer, E. (2001). Single-molecule tracking of myosins with genetically engineered amplifier domains. *Nature Structural Biology, 8*, 226. doi:10.1038/84962

Sata, M., & Ikebe, M. (1996). Functional analysis of the mutations in the human cardiac beta-myosin that are responsible for familial hypertrophic cardiomyopathy. Implication for the clinical outcome. *The Journal of Clinical Investigation, 98*(12), 2866-2873. doi:10.1172/JCI119115

Schwartz, K., Lecarpentier, Y., Martin, J. L., Lompré, A. M., Mercadier, J. J., & Swynghedauw, B. (1981). Myosin isoenzymic distribution correlates with speed of myocardial contraction. *Journal of molecular and cellular cardiology, 13*(12), 1071-1075. doi:10.1016/0022-2828(81)90297-2

Seidman, C. E., & Seidman, J. G. (2011). Identifying sarcomere gene mutations in hypertrophic cardiomyopathy: a personal history. *Circulation research, 108*(6), 743-750. doi:10.1161/CIRCRESAHA.110.223834

Seidman, C. E., & Seidman, J. G. (2014). Hypertrophic Cardiomyopathy. In A. L. Beaudet, B. Vogelstein, K. W. Kinzler, S. E. Antonarakis, A. Ballabio, K. M. Gibson, & G. Mitchell (Eds.), *The Online Metabolic and Molecular Bases of Inherited Disease*. New York, NY: The McGraw-Hill Companies, Inc.

Sieck, G. C., Ferreira, L. F., Reid, M. B., & Mantilla, C. B. (2013). Mechanical properties of respiratory muscles. *Comprehensive Physiology, 3*(4), 1553-1567. doi:10.1002/cphy.c130003

Sorajja, P., Nishimura, R. A., Gersh, B. J., Dearani, J. A., Hodge, D. O., Wiste, H. J., & Ommen, S. R. (2009). Outcome of Mildly Symptomatic or Asymptomatic Obstructive

Hypertrophic Cardiomyopathy: A Long-Term Follow-Up Study. *Journal of the American College of Cardiology, 54*(3), 234-241. doi:10.1016/j.jacc.2009.01.079

Spudich, J. A. (2014). Hypertrophic and dilated cardiomyopathy: four decades of basic research on muscle lead to potential therapeutic approaches to these devastating genetic diseases. *Biophysical Journal, 106*(6), 1236-1249. doi:10.1016/j.bpj.2014.02.011

Spudich, J. A., Huxley, H. E., & Finch, J. T. (1972). Regulation of skeletal muscle contraction: II. Structural studies of the interaction of the tropomyosin-troponin complex with actin. *Journal of Molecular Biology, 72*(3), 619-632. doi:10.1016/0022-2836(72)90180-5

Stassijns, G., Gayan-Ramirez, G., De Leyn, P., de Bock, V., Dom, R., Lysens, R., & Decramer, M. (1999). Effects of dilated cardiomyopathy on the diaphragm in the Syrian hamster. *European Respiratory Journal, 13*(2), 391-397.

Stassijns, G., Gayan-Ramirez, G., De Leyn, P., Verhoeven, G., Herijgers, P., De Bock, V., . . . Decramer, M. (1998). Systolic ventricular dysfunction causes selective diaphragm atrophy in rats. *American journal of respiratory critical care medicine, 158*(6), 1963-1967.

Stein, L. A., Chock, P. B., & Eisenberg, E. (1984). Rate-limiting step in the actomyosin adenosine triphosphatase cycle. *Biochemistry, 23*(7), 1555-1563. doi:10.1021/bi00302a033

Stein, L. A., Schwarz, R. P., Chock, P. B., & Eisenberg, E. (1979). Mechanism of the actomyosin adenosine triphosphatase. Evidence that adenosine 5'-triphosphate hydrolysis can occur without dissociation of the actomyosin complex. *Biochemistry, 18*(18), 3895-3909. doi:10.1021/bi00585a009

Sugiura, S., Kobayakawa, N., Fujita, H., Momomura, S. I., Chaen, S., & Sugi, H. (1998). Distinct Kinetic Properties of Cardiac Myosin Isoforms Revealed by In Vitro Studies. *Advances in experimental medicine and biology, 453*, 125-130. doi:10.1007/978-1-4684-6039-1_15

Sugiura, S., Kobayakawa, N., Fujita, H., Yamashita, H., Momomura, S.-i., Chaen, S., . . . Sugi, H. (1998). Comparison of Unitary Displacements and Forces Between 2 Cardiac Myosin Isoforms by the Optical Trap Technique. *Circulation research, 82*(10), 1029-1034. doi:doi:10.1161/01.RES.82.10.1029

Supinski, G., DiMarco, A., & Dibner-Dunlap, M. (1994). Alterations in diaphragm strength and fatiguability in congestive heart failure. *Journal of Applied Physiology, 76*(6), 2707-2713. doi:10.1152/jappl.1994.76.6.2707

Sweeney, H. L., Straceski, A. J., Leinwand, L. A., Tikunov, B. A., & Faust, L. (1994). Heterologous expression of a cardiomyopathic myosin that is defective in its actin interaction. *Journal of Biological Chemistry, 269*(3), 1603-1605.

Sweeney, H. L., & Stull, J. T. (1990). Alteration of cross-bridge kinetics by myosin light chain phosphorylation in rabbit skeletal muscle: implications for regulation of actin-myosin interaction. *Proceedings of the National Academy of Sciences of the United States of America, 87*(1), 414-418. doi:10.1073/pnas.87.1.414

Sys, S., Housmans, P., Van Ocken, E., & Brutsaert, D. J. P. A. (1984). Mechanisms of hypoxia-induced decrease of load dependence of relaxation in cat papillary muscle. *Pflügers Archiv - European Journal of Physiology, 401*(4), 368-373.

Tardiff, J. C., Factor, S. M., Tompkins, B. D., Hewett, T. E., Palmer, B. M., Moore, R. L., . . . Leinwand, L. A. (1998). A truncated cardiac troponin T molecule in transgenic mice

suggests multiple cellular mechanisms for familial hypertrophic cardiomyopathy. *The Journal of Clinical Investigation, 101*(12), 2800-2811. doi:10.1172/JCI2389

Tikunov, B. A., Mancini, D., & Levine, S. (1996). Changes in Myofibrillar Protein Composition of Human Diaphragm Elicited by Congestive Heart Failure. *Journal of molecular and cellular cardiology, 28*(12), 2537-2541. doi:10.1006/jmcc.1996.0245

Topol, E. J., Traill, T. A., & Fortuin, N. J. (1985). Hypertensive Hypertrophic Cardiomyopathy of the Elderly. *New England Journal of Medicine, 312*(5), 277-283. doi:10.1056/nejm198501313120504

Van Buren, P., Harris, D. E., Alpert, N. R., & Warshaw, D. M. (1995). Cardiac V1 and V3 myosins differ in their hydrolytic and mechanical activities in vitro. *Circulation research, 77*(2), 439-444.

van Hees, H. W., van der Heijden, H. F., Ottenheijm, C. A., Heunks, L. M., Pigmans, C. J., Verheugt, F. W., . . . Dekhuijzen, P. N. (2007). Diaphragm single-fiber weakness and loss of myosin in congestive heart failure rats. *American journal of physiology. Heart and circulatory physiology, 293*(1), H819-828. doi:10.1152/ajpheart.00085.2007

Velden, J. v. d., & Stienen, G. J. M. (2019). Cardiac Disorders and Pathophysiology of Sarcomeric Proteins. *Physiological Reviews, 99*(1), 381-426. doi:10.1152/physrev.00040.2017

Vikstrom, K. L., Factor, S. M., & Leinwand, L. A. (1996). Mice expressing mutant myosin heavy chains are a model for familial hypertrophic cardiomyopathy. *Molecular medicine (Cambridge, Mass.), 2*(5), 556-567.

Walker, J. S., Li, X., & Buttrick, P. M. (2010). Analysing force–pCa curves. *Journal of Muscle Research- Cell Motility, 31*(1), 59-69. doi:10.1007/s10974-010-9208-7

Wang, K., McCarter, R., Wright, J., Beverly, J., & Ramirez-Mitchell, R. (1991). Regulation of skeletal muscle stiffness and elasticity by titin isoforms: a test of the segmental extension model of resting tension. *Proceedings of the National Academy of Sciences, 88*(16), 7101-7105. doi:10.1073/pnas.88.16.7101

Wang, K., & Ramirez-Mitchell, R. (1983). A network of transverse and longitudinal intermediate filaments is associated with sarcomeres of adult vertebrate skeletal muscle. *The Journal of cell biology, 96*(2), 562-570.

Weber, A., & Murray, J. M. (1973). Molecular control mechanisms in muscle contraction. *Physiological Reviews, 53*(3), 612-673. doi:10.1152/physrev.1973.53.3.612

Widmaier, E. P., Raff, H., & Strang, K. T. (2006). *Vander's human physiology: the mechanisms of body function*. Boston: McGraw-Hill Higher Education.

Witt, C., Borges, A., Haake, H., Reindl, I., Kleber, F., & Baumann, G. (1997). Respiratory muscle weakness and normal ventilatory drive in dilative cardiomyopathy. *European Heart Journal, 18*, 1322-1328. doi:10.1093/oxfordjournals.eurheartj.a015445

Yang, Q., Sanbe, A., Osinska, H., Hewett, T. E., Klevitsky, R., & Robbins, J. (1998). A mouse model of myosin binding protein C human familial hypertrophic cardiomyopathy. *The Journal of Clinical Investigation, 102*(7), 1292-1300. doi:10.1172/JCI3880